九州大学学術情報リポジトリ
Kyushu University Institutional Repository

Studies on the influence of competitive nonradiative processes on triplet harvesting applications

能塚, 直人

https://doi.org/10.15017/4060119

出版情報：九州大学, 2019, 博士（工学）, 課程博士
バージョン：
権利関係：

2020

Doctoral thesis

Studies on the influence of competitive nonradiative processes on triplet harvesting applications

Naoto Notsuka

Department of Chemistry and Biochemistry

Graduate School of Engineering

Kyushu University

Table of Contents

Chapter 1

Introduction

1. 1. Background

1. 1. 1. Organic light emitting devices (OLEDs)

Because we live in a society where electrical infrastructure has been well-developed, applications run by electricity are essential to our daily life. As an amount of communication traffic increases year by year,[1] display devices are desired to extend their presence to unconventional places such as blank walls, glasses,[2] and body surfaces.[3] Organic devices have high potential for such kinds of applications because of their flexibilities.

Organic electroluminescence (EL) was first reported from an anthracene crystal with the thickness of dozens of micrometers by applying extraordinary high voltage such as 1000 V in 1963.[4] After the single crystal studies, various thin film devices had been examined in 1970th to 1980th[5] and in 1987, C. W. Tang reported an impressive bilayer organic light-emitting diode (OLED),[6] demonstrating ~1000 cd m^{-2} with a low driving voltage of 5 V. After this report, the OLEDs have attracted extensive attention for display and lighting applications because of their unique characteristics such as mechanical flexibility, transparency, and solution processability in addition to the high EL efficiency[7] Moreover, high contrast and fast response are suitable for use in displays and large-area surface emission is suitable for use in

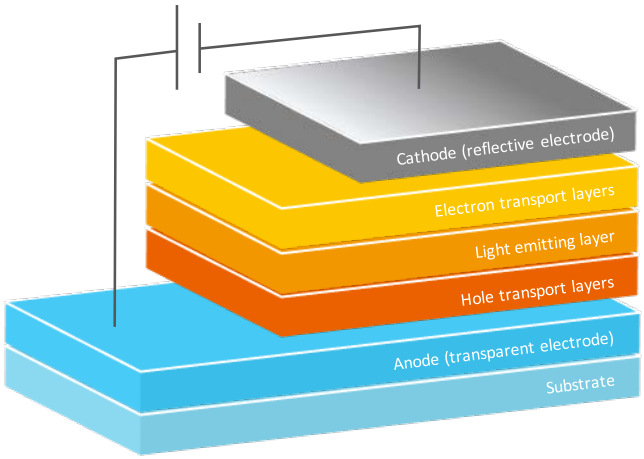

Figure 1-1. Illustration of a basic three-layer OLED.

lighting applications.[8]

Nowadays, flat or flexible panel displays utilizing OLEDs have been popular and the market has been rapidly expanding.[9] **Figure 1-1** shows one of the basic OLED structures, called a bottom-emission type OLED. This bottom type device archetecuture has been commonly used at laboratory scale because of its easy-to-fabrication. The OLEDs consist of stacked thin uniform layers with the thickness of equal to or less than sub-micrometers to produce EL with practicable driving voltage, even though organic amorphous films have low charge carrier mobilities of about 10^{-3}–10^{-5} cm^2 V^{-1} s^{-1}.[10] OLEDs show light emission when electrically generated excitons deactivate to the grand state from the excited states. The excitons are generated by the reconbination of electron-hole pairs injected from an anode and a cathode, respectively. To obtain efficient luminescence from a light emitting layer, the structure of OLEDs has been developed to incorporate various functional layers. Generally, a hole transporting and an electon transporting layers adjacent to the light-emitting layer are formed to transport charge carriers from the electrodes to the emitting layer.[11] To confine charge carriers and excitons in the emitting layer, blocking layers are also inserted between the emitting layer and the transporting layers.[12,13] Moreover, carrier injection layers, inserted at the interfaces between transporting layers and electrodes, help reducing the driving voltage of the devices.[14] Further, in the light emitting layer, a host-guest system, dispersing emitters into a host matrix, can be introduced to improve efficiency.[15] Insufficient energy confinement resulting from the mismatched energy difference between the emitter and the host or the adjacent layers causes unexpected exciton deactivation.[16] Therefore, the host matrices and adjacent layers should have higher energy gap than that of the emitter. The host is also required to have a good spectral overlap between the emission of the host and the

absorption of the guest molecule to induce efficient energy transfer to guest materials.[17] Applying bipolar carrier transportability to host matrices by mixing two or more types of materials also helps achieving ideal bipolar carrier transport and successive carrier recombination.[18] Furthermore, the encapsulation of OLEDs with inert gas is favorable to prevent undesired reactions with the atmospheric constituents.[19]

1. 1. 2. Parameters of light emitting performances and decay rate constants of excitons

When an electronically excited organic molecule relaxes, the relaxation processes are divided into two types. A process with light emission is called as a "radiative" decay process and the process without emission is called a "nonradiative" decay process. The total exciton decay rate constant k_{total}, which means transition probabilities per time from excited states, is the sum of the individual rate constants of all decay channels as below:

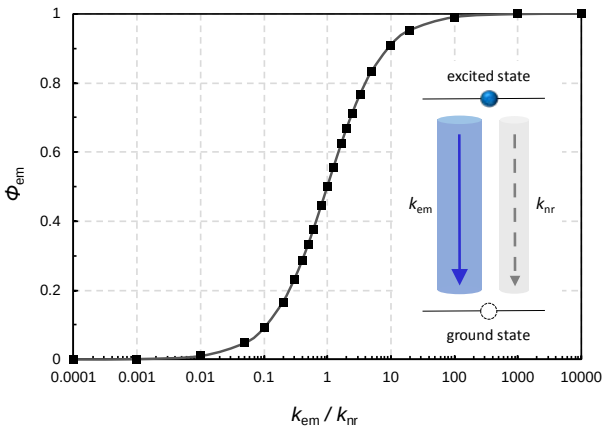

Figure 1-2. The relationship between Φ_{em} and k_{em}/k_{nr}. Inset: Illustration of the relaxation process of an exciton.

$$k_{total} = k_1 + k_2 + \ldots + k_n = \Sigma\, k_i \,. \qquad (1\text{-}1)$$

An exciton decay lifetime (τ) and a quantum yield (Φ) of a certain pathway of the molecules are connected to the rate constants.

$$\tau = 1 / k_{total} = 1 / (k_{em} + k_{nr}) \,, \qquad (1\text{-}2)$$

$$\Phi = k / k_{total} = k / \Sigma\, k_i = k / \tau \,. \qquad (1\text{-}3)$$

Here, the relationship between an emission efficiency (Φ_{em}) and a ratio of the rate

constants of radiative (k_{em}) and nonradiative decay processes (k_{nr}) is illustrated in **Figure 1-2**.

$$\Phi_{em} = k_{em} / (k_{em} + k_{nr}) = k_{em} / \tau \, . \quad (1\text{-}4)$$

The rate constants of organic emitters are one of the fundamental indicators for evaluating exciton dynamics, photoluminescence (PL) and EL performances. Understanding of exciton dynamics in emissive organic materials is essential for the development of high-performance organic light-emitting applications such as OLEDs,[20] bioimaging probes,[21] and organic long-persistent luminescence.[22]

1. 1. 3. Spin formation and exciton harvesting in OLEDs

A possible electron spin multiplicity of excitons, *M*, resulted from bimolecular reactions between different species is expressed as below:[23]

$$M = 2S + 1 \, , \quad (1\text{-}5)$$

where *S* is the total spin angular momentum of unpaired electrons (± 1/2) of excitons. The reaction between different species, A and B, through an encounter complex is expressed,

$$^{m}\mathrm{A} + {}^{n}\mathrm{B} \rightleftarrows mn\,(\mathrm{AB}) \rightarrow \mathrm{Product} \, , \quad (1\text{-}6)$$

where *m* and *n* represent the spin multiplicity of A and B, respectively, and the product *mn* gives the number of possible spin states of the encounter-pair AB. Because two doublets, hole and electron pair, recombine in the emitting layer of OLEDs, the exciton can be formed as four types of pair states, one is a singlet and other three are triplets. Because three-quarters of electrically generated excitons are directly formed in a triplet state, harvesting triplet excitons is crucial to enhance OLED efficiency.[24]

1. 1. 4. Triplet harvesting materials for OLEDs

Transition probabilities between different energy levels are controlled by the

production of three transition factors.[25]

$$\text{Total transition factor} \quad f = f_e \times f_v \times f_s , \tag{1-7}$$

where, f_e, f_v, and f_s represent transition factors based on an electronic factor, Franck-Condon (i.e., vibrational) factor, and spin factor, respectively. While the transition between a lowest excited single state (S_1) and a ground state (S_0) is strongly allowed, the transition between a lowest excited triplet state (T_1) and S_0 of pure organic aromatics are forbidden due to the small value of f_s. Thus, harvesting triplet excitons as light emission are not easy under normal conditions. However, the forbidden transitions become partially allowed by perturbations such as vibronic and spin-orbit coupling. Some organic aromatics are known to show phosphorescence with the transition from T_1 to S_0 at low temperature.[26] Since the nonradiative deactivation factors of triplet excitons are easily suppressed at low temperatures, the slow radiative process of phosphorescence can exceed the nonradiative deactivation pathway, resulted in the appearance of phosphorescence emission.

Generally, the phosphorescence emission decreases with increasing temperature (T) because the temperature-dependent k_{nr} from T_1 ($k_{nr}^T(T)$) becomes larger than the rate constant of phosphorescence (k_{phos}). Therefore, most aromatic molecules show no room-temperature phosphorescence (RTP). Therefore, to observe RTP from organic molecules, k_{phos} should be larger than k_{nr}^T at room temperature (k_{nr}^T(RT)).

One effective approach for harvesting triplet excitons as emission is the enhancement of k_{phos}. Introducing heavy atoms like bromine,[27] iridium,[28] and platinum[29] enhances both ISC and k_{phos} through the spin-orbit coupling due to “heavy atom effect” which is proportional to the fourth power of the number of nuclear charges (Z). So far, such a mechanism has been adopted to practical OLEDs to maximize internal quantum

efficiency[28b] and in fact $Ir(ppy)_3$ derivatives have been widely used for display applications.[30] In this case, the materials are designed to be shortened the exciton lifetime to the order of micro-second. However, there some critical issues to overcome for these emitters. A decrease of EL efficiency at high brightness, called “roll-off”, results from exciton-exciton and exciton-polaron annihilations is caused by the accumulation of triplet excitons.[31] Further, exciton reactivity leads to luminance degradation of OLEDs,[32] which is especially critical in highly excited energy regions, i.e., blue emitters, because decomposition of materials and the successive exciton quenching by the decomposed products are likely to occur.[33,34]

Therefore, recent advanced OLEDs often contain blue subpixels based on triplet-triplet annihilation or fusion (TTA/TTF) emitters, which can improve the efficiency with the enhancement of the device stability.[35] According to **Schemes (1-5)** and **(1-6)**, two encountered triplets can produce nine different configurations of the encounter-pair, one is a singlet, three are triplets and five are quintets.

$$^3M^* + {}^3M^* \rightleftarrows {}^5(M \cdots M)^* \quad (1\text{-}8)$$

$$\rightleftarrows {}^3(M \cdots M)^* \rightarrow {}^3M^* + {}^1M \quad (1\text{-}9)$$

$$\rightleftarrows {}^1(M \cdots M)^* \rightarrow {}^1M^* + {}^1M \quad (1\text{-}10)$$

Generated singlet contributes to fluorescence and generated triplets can be recycled into these processes. As a result, 15% more singlets can be generated, in addition to 25% of originally generated singlet excitons.[35a]

Recently, effective electron-photon conversion has also been achieved by thermally activated delayed fluorescent (TADF) emitters.[36-38] The TADF mechanism, which was firstly discovered in Eosin Y[39] had been significantly developed to aim for electrical excitation,[36] resulted in ultimate efficiency.[37] In fact, an endothermic intersystem crossing

pathway from T_1 to S_1 (reverse intersystem crossing, RISC), led to delayed fluorescence, resulted in the harvesting triplet excitons under room temperature with nearly 100%.[38] The relationship between k_{risc} and ΔE_{ST} shows an exponential relationship.

$$k_{risc} \propto A \times \exp(-\Delta E_{ST} / k_B T), \quad (1\text{-}11)$$

where A is a pre-factor, ΔE_{ST} is the energy gap between S_1 and T_1, and k_B is a Boltzmann constant. For designing efficient TADF emitters, the energy difference (ΔE_{ST}) between S_1 and T_1 should be minimized to accelerate k_{risc}.

1. 1. 5. Suppression of nonradiative deactivation pathways

Suppression of a nonradiative deactivation pathway also contributes to improve Φ_{em} and this idea can be useful not only for OLEDs,[40] but also for various applications such as long-lived room temperature phosphorescence (LL-RTP),[22a] TTA upconversion,[41] and optical gas sensors.[42]

EL from OLEDs containing carbonyl compounds as a phosphorescent emitter driven under low temperature had been reported.[43] However, the OLEDs required high driving voltage under the low temperature at which k_{phos} can compete with $k_{nr}^{T}(T)$, because charge carrier mobilities in organic semiconductors strongly depends on temperature due to their thermally activated hopping conduction mechanism.[44]

The total $k_{nr}^{T}(T)$ of emitting materials can be divided into two components of an internal factor ($k_{nr,int}^{T}(T)$) and an external factor ($k_{nr,ext}^{T}(T)$).[22a]

$$k_{nr}^{T}(T) = k_{nr,int}^{T}(T) + k_{nr,ext}^{T}(T). \quad (1\text{-}12)$$

The rate constant $k_{nr,int}^{T}(T)$ is related to the product of f_e, f_v, and f_s. Here, f_v corresponds to the square of the vibrational overlap of initial and final states, showing an exponential relationship with the energy gap between the states (ΔE):[45]

$$f_v \propto \exp(-\Delta E)\ . \tag{1-13}$$

Generally, high-frequency C-H stretching vibration strongly affects f_v and the substitution of the hydrogen atom by deuterium can reduce this value.[46] This can be explained by the relationship between an energy gap between the vibrionic states (ΔE_{vib}) and effective mass (m_{eff}), which is increased by deuteration.

$$\Delta E_{vib} \propto m_{eff}^{-1/2}\ , \tag{1-14}$$

$$m_{eff} = m_H m_C / (m_H + m_C)\ . \tag{1-15}$$

Since deuteration greatly affects m_{eff}, ΔE_{vib} becomes smaller and the number of vibrational quanta (v) of S_0, reaching to T_1, increases. At higher v value, the overlap integral of the two states decreases due to an increase of the number of nodes in the wavefunction, resulting in the cancellation of the positive and negative contributions (**Figure 1-3**).

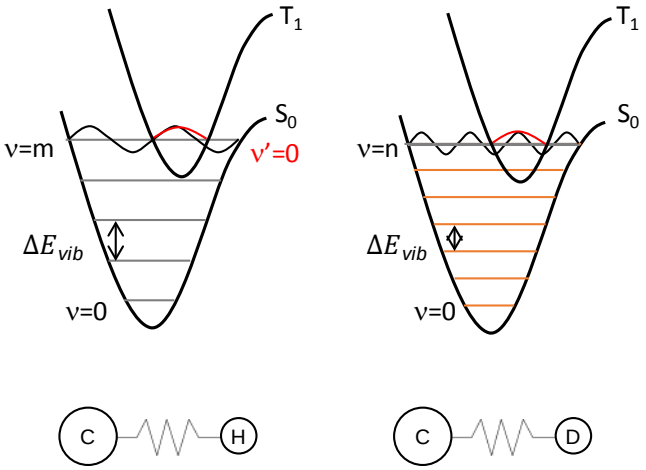

Figure 1-3. Schematic illustration of the deuteration effect. Franc-Condon factor of C-D (right) is smaller than that of C-H (left).

The rate constant, $k_{nr,ext}^T(T)$, can be further divided into several factors (**Figure 1-4**), for example, aggregation induced quenching caused by oxygen quenching ($k_{q,O2}^T(T)$),[47] concentration quenching or phase separation ($k_{AIQ}^T(T)$),[48] energy transfer from the triplet energy level of emitters to the triplet energy level of energy acceptors ($k_{ET}^T(T)$)[16] and diffusional motion of the matrix ($k_{diff}^T(T)$),[22a]

$$k_{nr,ext}^T(T) = k_{q,O2}^T(T) + k_{AIQ}^T(T) + k_{ET}^T(T) + k_{diff}^T(T) + \ldots\ . \tag{1-16}$$

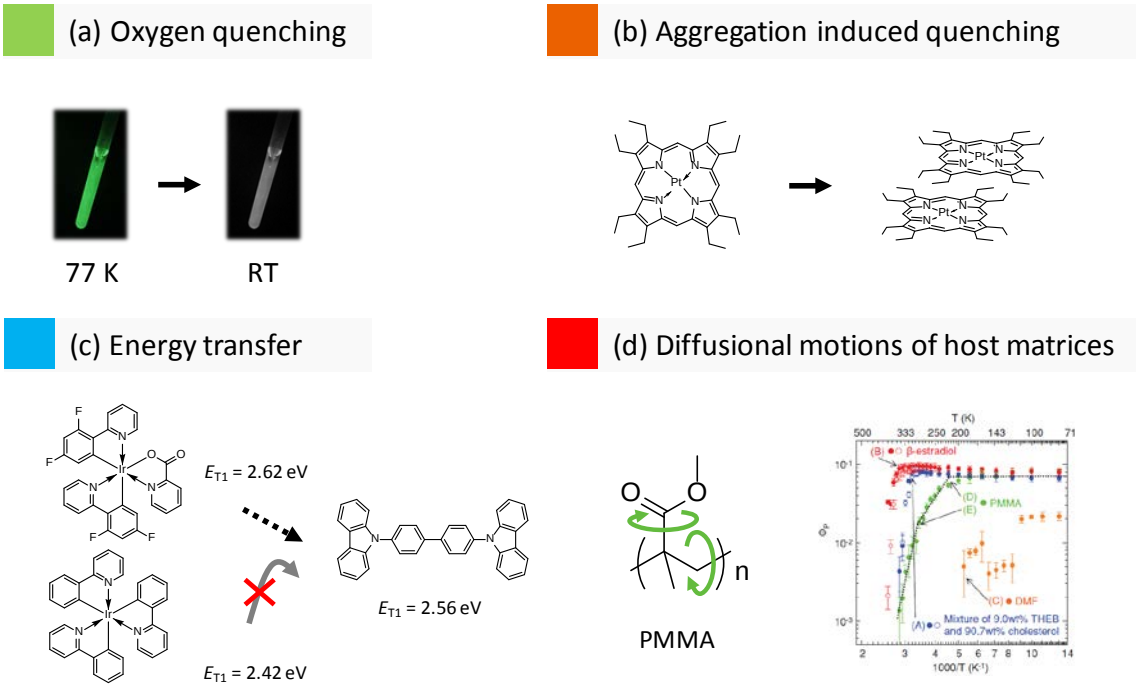

Figure 1-4. Schematic illustration of the nonradiative deactivation factors of triplets caused by a) oxygen quenching, b) aggregation induced quenching, c) energy transfer, and d) diffusional motion of the host matrices.

In solution, $k_{q,O2}^{T}$ can be predominant over other deactivation pathways even though Ir based complexes are used as an emitter.[49] Molecular oxygen (O_2) is well-known to quench triplet emitters easily because O_2 has a low-lying singlet excited state from a ground triplet state.[50] In other words, triplet generators, especially from photo-excitation, can provide effective sensitizers for singlet oxygen.[51] Many studies about RTP support that O_2 quenching plays a critical role in the vanishment of phosphorescence.[22a,25] Further, in solid states films used in OLEDs, k_{AIQ}^{T} (T) can be kept to be a smaller value when the emitter is doped in a host matrix at a low concentration of 0.5 ~ 2 mol%. On the other hand, at the high concentration of emitter molecules or a phase separated condition between emitter molecules and host matrices, it results in exciton-exciton annihilation or aggregation induced low-energy lying excimer formation. In addition, k_{ET}^{T} (T) becomes larger when impurities contaminated during manufacturing processes or fabrication

procedures present nearby the emitting molecules. In phosphorescence based OLEDs, the incomplete device structures having host matrices or carrier transport layers with low T_1 energy also cause endothermic energy transfer under room temperature.[16] Further, thermally diffusional motions of host matrices, leading to an enhancement of k_{diff}^{T} (T), also reported to quench triplet excitons with increasing the temperature.[22a]

1. 2. Purpose and outline of this study

The purpose of this thesis is understanding the nonradiative decay processes of excited states aimed for triplet harvesting as light emission and their applications.

When evaluating the photophysical characteristics of molecules, k_{em} can directly reflect the probability of a radiative transition from the lowest excited state to the ground state, S_0, whereas k_{nr} is represented as the sum of the remaining non-radiative electron-transition probabilities. In case of deriving deactivation rate constants only from optical measurements, although various types of noncoupled paths, such as vibration-induced quenching, concentration quenching, and energy transfer should be considered, k_{nr} cannot be decomposed into each component. As mentioned above, when k_{nr} is large enough to compete with k_{em}, clarification of the dominant factor of k_{nr} and its suppression is crucial to improve the light-emission abilities of emitters. In particular, triplet excitons are sensitive for nonradiative events and are easily quenched because k_{phos} or k_{risc} is normally much smaller than k_{nr}^{T} because of the spin-forbidden nature of the transition at room temperature. **Figure 1-5** and **Table 1-1** summarize the activation and deactivation processes in organic molecules focused in this study.

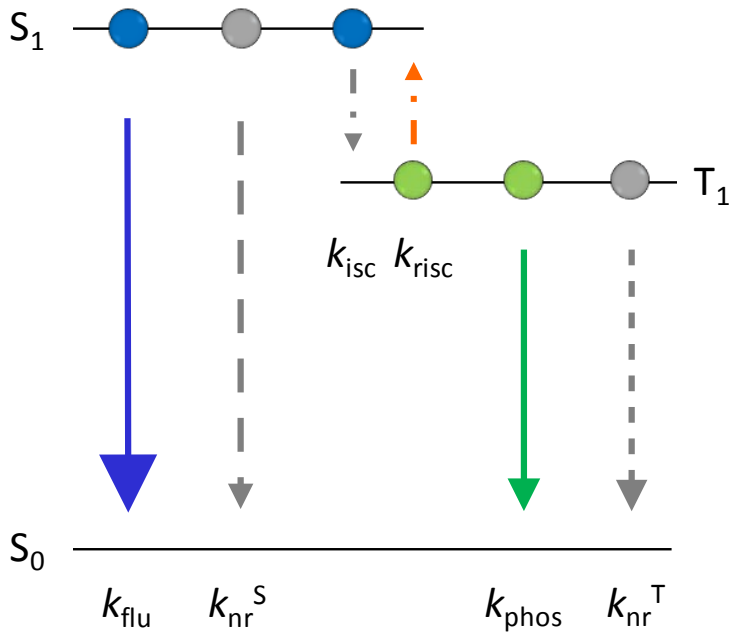

Figure 1-5. Schematic illustration of activation and deactivation processes in organic molecules.

Table 1-1. Summary of transition rate constants in this study.

Rate constant	Initial state	Final state	Light radiation	Triplet harvesting in OLEDs
k_{flu}	S_1	S_0	✓	
k_{phos}	T_1	S_0	✓	✓
k_{isc}	S_1	T_0		
k_{risc}	T_1	S_1		✓
k_{nr}^S	S_1	S_0		
k_{nr}^T	T_1	S_0		

In Chapter 2, I demonstrated long-lived phosphorescence at room temperature (LL-RTP) resulting from the suppression of the nonradiative deactivation of triplet excitons in conventional organic semiconducting host–guest systems (**Figure 1-5**). The nonradiative deactivation pathway strongly depends on the triplet energy gap between the guest emitting molecules and the host matrices ($\Delta E_{T1\text{-}T1'}$). The triplet energy gap required to confine the long-lived triplet excitons (~0.5 eV) is much larger than that of conventional host–guest systems for room temperature phosphorescent emitters. By effectively confining triplet excitons, I demonstrate long-lived room temperature phosphorescence under both optical and electrical excitation.

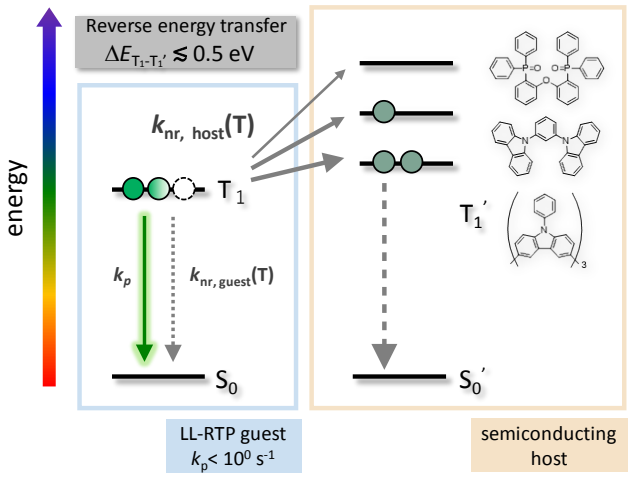

Figure 1-5. Schematic illustration of Chapter 2. Investigating the dominant quenching factor in afterglow OLEDs.

In Chapter 3, I investigated nonradiative decay behavior, including internal and external exciton quenching processes of various types of TADF materials in solution (**Figure 1-6**). Under air-saturated conditions, both the lowest singlet and triplet excited states of almost all TADF materials

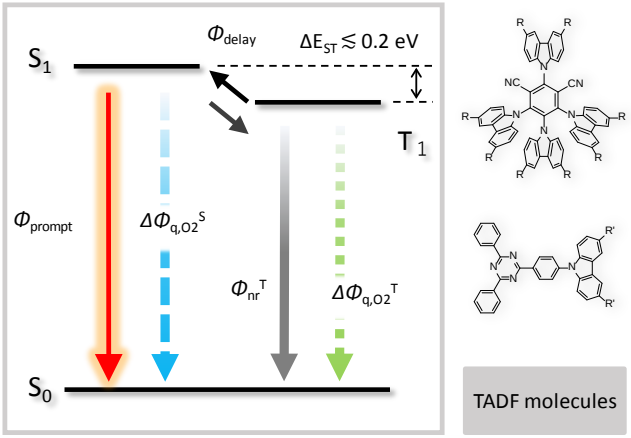

Figure 1-6. Schematic illustration of Chapter 3. Investigating quenching pathways of TADF.

showed oxygen quenching. I carefully studied the effect of oxygen quenching for both singlet and triplet spin states to develop a method for determination of the triplet contribution to the total photoluminescence quantum yield from the transient photoluminescence profiles. Furthermore, I observed a clear energy gap law for the internal nonradiative processes.

Finally, in Chapter 4, the thesis is summarized and prospects are discussed.

1. 3. References

[1] Cisco Visual Networking Index: Forecast and Trends, 2017–2022 White Paper. **2019**.

[2] G. Gu, V. Bulovic, P. E. Burrows, S. R. Forrest, M. E. Thompson, *Appl. Phys. Lett.* **1996**, *68*, 2606.

[3] J. A. Rogers, T. Someya, Y. Huang, *Science* **2010**, *327*, 1603.

[4] M. Pope, H. P. Kallmann, P. Magnante, *J. Chem. Phys.* **1963**, *38*, 2042.

[5] C. W. Tang, S. A. VanSlyke, *Appl. Phys. Lett.* **1987**, *51*, 913.

[6] a) P. S. Vincett, W. A. Barlow, R. A. Hann, G. G. Roberts, *Thin Solid Films* **1982**, *94*, 171; b) S. Hayashi, E. Etoh S. Saito, *Jpn. J. Appl. Phys.* **1986**, *25*, L773.

[7] J. H. Burroughes, D. D. C. Bradley, A. R. Brown, R. N. Marks, K. Mackay, R. H. Friend, P. L. Burns, A. B. Holmes, *Nature* **1990**, *347*, 539.

[8] T. Tsujimura, OLED Display Fundamentals and Applications, Second Edition, John Wiley & Sons, Inc. **2017**.

[9] R. Young, *Inform. Disp.* **2019**, *35*, 24.

[10] R. G. Kepler, P. M. Beeson, S. J. Jacobs, R. A. Anderson, M. B. Sinclair, V. S. Valencia, P. A. Cahill, *Appl. Phys. Lett.* **1995**, *66*, 3618.

[11] C. Adachi, S. Tokito, T. Tsutsui, S. Saito, *Jpn. J. Appl. Phys.* **1988**, *27*, L269.

[12] D. F. O'Brien M. A. Baldo, *Appl. Phys. Lett.* **1999**, 74, 442.

[13] T. Noda, H. Ogawa, Y. Shirota, *Adv. Mater.* **1999**, *11*, 283.

[14] a) Y. Shirota, Y. Kuwabara, H. Inada, T. Wakimoto, H. Nakada, Y. Yonemoto, S. Kawami, K. Imai, *Appl. Phys. Lett.* **1994**, *65*, 807; b) S. A. VanSlyke, C. H. Cheng, C. W. Tang, *Appl. Phys. Lett.* **1996**, *69*, 2160.

[15] C. W. Tang, S. A. VanSlyke, C. H. Cheng, *Appl. Phys. Lett.* **1989**, *65*, 3160.

[16] a) R. J. Holmes, B. W. D'Andrade, S. R. Forrest, X. Ren, J. Li, M. E. Thompson, *Appl. Phys. Lett.* **2003,** *83*, 3818; b) M. A. Baldo, S. R. Forrest, *Phys. Rev. B* **2000**, *62*, 10958; c) F. C. Chen, G. F. He, Y. Yang, *Appl. Phys. Lett.* **2003**, *82*, 1006; d) K. Goushi, R. Kwong, J. J. Brown, H. Sasabe, C. Adachi, *J. Appl. Phys.* **2004**, *95*,

7798.

[17] T. Förstor, *Ann. Phys.* **1948**, *2*, 55.

[18] A. B. Chwang, R. C. Kwong, J. J. Brown, *Appl. Phys. Lett.* **2002**, *80*, 725.

[19] J. McElvain, H. Antoniadis, M. R. Hueschen, J. N. Miller, D. M. Roitman, J. R. Sheats, R. L. Moon, *J. Appl. Phys.* **1996**, *80*, 6002.

[20] a) T. Tsutsui, S. Saito, Organic Multilayer-Dye Electroluminescent Diodes-Is There Any Difference with Polymer LED? Kluwer Academic, Dordrecht, **1993**. b) L. J. Rothberg, A. J. Lovinger, *J. Mater. Res.* **1996**, *11*, 3174.

[21] M. Y. Berezin, S. Achilefu, *Chem. Rev.* **2010**, *110*, 2641.

[22] a) S. Hirata, K. Totani, J. Zhang, T. Yamashita, H. Kaji, S. R. Marder, T. Watanabe, C. Adachi, *Adv. Funct. Mater.* **2013**, *23*, 3386; b) R. Kabe, C. Adachi, *Nature* **2017**, *550*, 384.

[23] D. H. Volman, G. S. Hammond, K. Gollnick, Advances in Photochemistry Volume 14, A Wiley-Interscience Publication, **1988**.

[24] A. R. Brown, K. Pichler, N. C. Greenham, D. D. C. Bradley, R. H. Friend, A. B. Holmes, *Chem. Phys. Lett.* **1993**, *210*, 61.

[25] N. J. Turro, V. Ramamurthy, J. C. Scaiano, Modern Molecular Photochemistry of Organic Molecules. University Science Books, **2010**.

[26] S.P. McGlynn, T. Azumi, M. Kinoshita, Molecular spectroscopy of the triplet state. Prentice-Hall, **1969.**

[27] O. Bolton, K. Lee, H. J. Kim, K. Y. Lin, J. Kim, *Nat. Chem.*, **2001**, *3*, 205.

[28] a) M. A. Baldo, S. Lamansky, P. E. Burrows, M. E. Thompson, S. R. Forrest, *Appl. Phys. Lett.* **1999**, *75*, 4; b) C. Adachi, M. A. Baldo, M. E. Thompson, S. R. Forrest, *J. Appl. Phys.* **2001**, *90*, 5048.

[29] M. A Baldo, D. F. O'Brien, Y. You, A. Shoutstikov, S. Sibley, M. E. Thompson, S. R. Forrest, *Nature* **1998**, *395*, 151.

[30] P. Semensa, *Inform. Disp.* **2013**, *29*, 26.

[31] N. C. Giebink and S. R. Forrest, *Phys. Rev. B* **2008**, *77*, 235215.

[32] P. E. Burrows, S. R. Forrest, T. X. Zhou, L. Michalski, *Appl. Phys. Lett.* **2000**, *76*, 2493.

[33] S. Schmidbauer, A. Hohenleutner, B. König, *Adv.Mater.* **2013**, *25*, 2114.

[34] N. Lin, J. Qiao, L. Duan, L. Wang, Y. Qiu, *J. Phys. Chem. C* **2014**, *118*, 7569.

[35] a) W. Helfrich, W. G. Schneider, *J. Chem. Phys.* **1966**, *44*, 2902. b) H. Kuma, C. Hosokawa, *Sci. Technol. Adv. Mater.* **2014**, *15*, 034201.

[36] A. Endo, M. Ogasawara, A. Takahashi, D. Yokoyama, Y. Kato, C. Adachi, *Adv. Mater.* **2009**, *21*, 480.

[37] a) A. Endo, K. Sato, K. Yoshimura, T. Kai, A. Kawada, H. Miyazaki, C. Adachi. *Appl. Phys. Lett*. **2011**, *98*, 083302; b) H. Tanaka, K. Shizu, H, Miyazaki, and C. Adachi, *Chem. Comm*. **2012**, *48*, 11392; c) S. Y. Lee, T. Yasuda, H. Nomura, C. Adachi, *Appl. Phys. Lett.* **2012**, *101*, 093306; d) K. Goushi, K. Yoshida, K. Sato, C. Adachi, *Nature Photon.* **2012**, *6*, 253; e) K. Sato, K. Shizu, K. Yoshimura, A. Kawada, H. Miyazaki, C. Adachi, *Phys. Rev. Lett.* **2013**, *110*, 247401.

[38] a) H. Uoyama, K. Goushi, K. Shizu, Hiroko Nomura, and C. Adachi, *Nature* **2012**, *492*, 234; b) S. Hirata, Y. Sakai, K. Masui, H. Tanaka, S. Y. Lee, H. Nomura, N. Nakamura, M. Yasumatsu, H. Nakanotani, Q. Zhang, K. Shizu, H. Miyazaki, C. Adachi, *Nature Mater.* **2015**, *14*, 330; c) Q. Zhang, B. Li, S. Huang, H. Nomura, H. Tanaka C. Adachi, *Nature Photon.* **2014**, *8*, 326.

[39] S. Boudin, *J. Chim. Phys*, **1930**, *27*, 285.

[40] J. P. Martins, P. Martín-Ramos, C. Coya, M. Ramos Sliva, M.E.S. Eusebio, A.D. Andrés, Á.L. Álvarez, J. Martín-Gil, *J. lumin.* **2015**, *159*, 17.

[41] A. Danos, R. W. MacQueen, Y. Yap Cheng, M. Dvořák, T. A. Darwish, D. R. McCamey, T. W. Schmidt, *J. Phys. Chem. Lett.* **2015**, *6*, 15, 3061.

[42] J Gregory, J. W., Asai, K., Kameda, M., Liu, T., & Sullivan, J. P. (2008). *Proc. of the IMecE, Part G: J. Aerospace Eng.* **2008**, *222*, 249.

[43] a) M. Morikawa, et al. *51th Fall meeting, Jpn. Soc. Appl. Phys.* 28a-BP-8; b) S. Hashimoto, H. Suzuki, *Appl. Phys. Lett.* **1996**, *69*, 224.

[44] a) R. Coehoorn, W. F. Pasveer, P. A. Bobbert, M. A. J. Michels *Phys. Rev. B* **2005**, *72*, 155206; b) N. F. Mott W. D. Twose, *Adv. Phys.* **1961**, *10*, 107; c) H. Bässler,

Phys. Stat. Sol. **1993**, *175*, 15.

[45] W. Siebrand, *J. Chem. Phys.* **1966**, *44*, 4055.

[46] W. Siebrand, *J. Chem. Phys.* **1967**, *47*, 2411.

[47] G. Mehes, H. Nomura, Q. Zhang, T. Nakagawa, C. Adachi, *Angew. Chem. Int. Ed.* **2012**, *51*, 11311.

[48] a) A. Weller, *Pure Appl. Chem.* **1968**, *16*, 115; b) Y. Kawamura, J. Brooks, J. J. Brown, H. Sasabe, C. Adachi, *Phys. Rev. Lett.* **2006**, *96*, 017404; c) B. D'Andrade S. R. Forrest, *Chem. Phys.* **2003**, *286*, 321.

[49] N. Hasebe, K. Suzuki, H. Horiuchi, H. Suzuki, T. Yoshihara, T. Okutsu, S. Tobita, *Anal. Chem.* **2015**, *87*, 2360.

[50] A. A. Krasnovsky, Jr., *Photochem. Photohiol.* **1979**, *29*, 29.

[51] J. N. Demas, E. W. Harris, R. P. McBride, *J. Am. Chem. Soc.* **1977**, *99*, 3547.

Chapter 2

Development of Afterglow OLEDs Utilizing Long-Lived Room Temperature Phosphorescent Emitters

"Afterglow Organic Light Emitting Diodes"
Ryota Kabe, Naoto Notsuka, Kou Yoshida, Chihaya Adachi,
Advanced Materials, **28**, 655-660, (2016).

"Confinement of Long-Lived Triplet Excitons in Organic Semiconducting Host-Guest Systems"
Naoto Notsuka, Ryota Kabe, Kenichi Goushi, Chihaya Adachi,
Advanced Functional Materials, **27**, 40, 1703902, (2017).

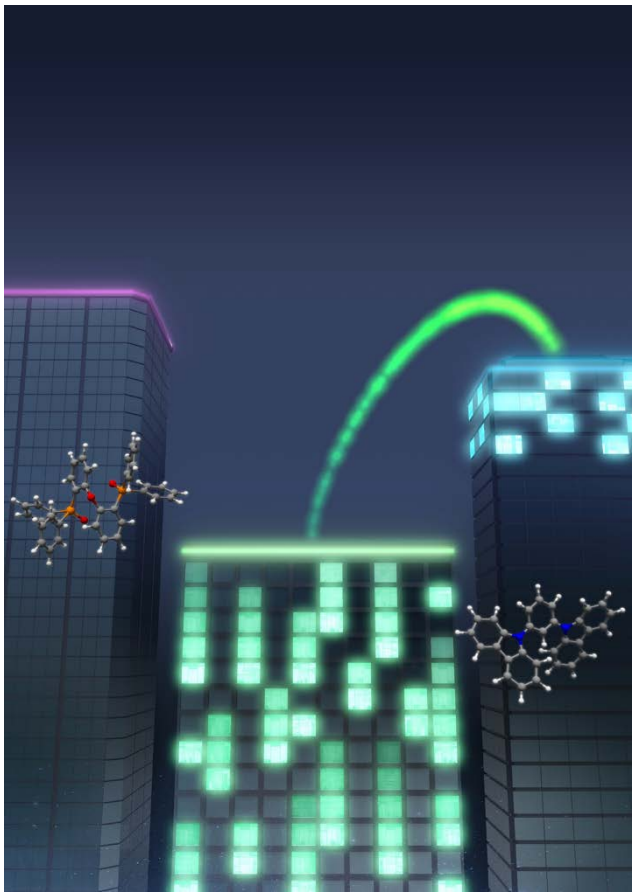

2. 1. Introduction of Chapter 2

Long persistent phosphors are widely commercialized as glow-in-the-dark paints for watches, indicators, emergency lights, and afterglow safety lamps and are being explored for use in *in vivo* bioimaging since the emission can be observed long after excitation.[1] Presently, this long-lasting emission is realized by an inorganic system of alkali aluminate (Sr, Al, O) doped with rare earths (Europium and Dysprosium),[2] which exhibits emission over 10 hours through the trapping and detrapping of photo-generated charge carriers. However, the inorganic phosphor alkali aluminate contains rare elements and requires very high fabrication temperatures over 1000 °C.[2] Moreover, this inorganic system requires photo-excitation in the ultraviolet region, the intensity of which is very weak in general modern lighting such as from light-emitting diodes (LEDs) and organic LEDs (OLEDs).

Some organic aromatics are also well-known to show long-lived emission called phosphorescence. While pure organic aromatic compounds have an intrinsically long phosphorescence lifetime exceeding a second, it is not obtained under conventional environmental conditions because of the presence of facile nonradiative deactivation processes from triplet states. Triplet excitons on organic molecules easily deactivate at room temperature because of the presence of thermally activated nonradiative pathways.

The approach for making RTP observable by the enhancement of k_{phos} as introduced in chapter 1, makes the emission lifetime is also very short. In contrast, minimization of k_{nr}^{T} (T) by using pure aromatic compounds and rigid host matrices also enables RTP. Many approaches, like host–guest systems,[3] clathrate compounds,[4] mixed crystals [5-6] and metal organic frameworks (MOFs),[7-8] have been reported. Because of the lack of enhancement of k_{phos}, this type of RTP persists for durations on the millisecond to second

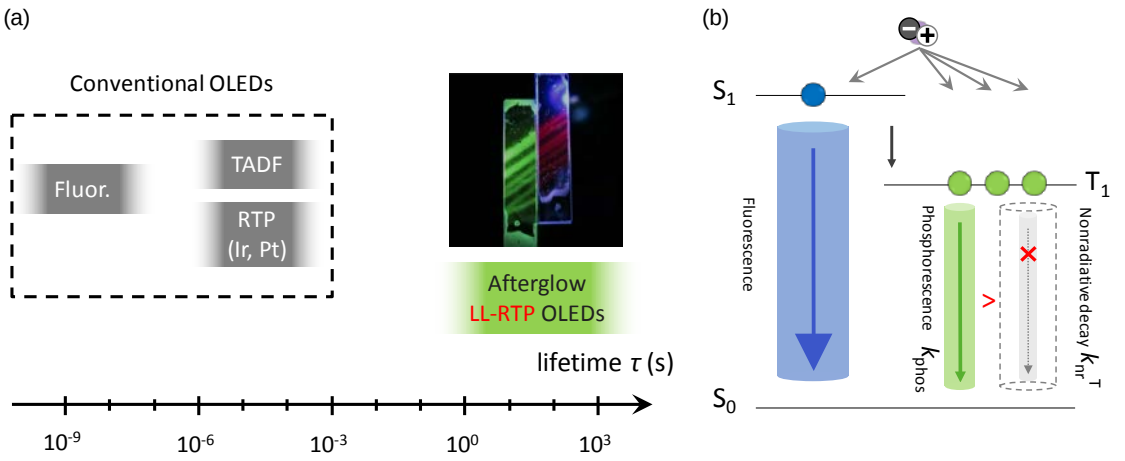

Figure 2-1. Conceptual illustration of afterglow OLEDs. a) Deactivation lifetimes compared between conventional OLEDs and afterglow OLEDs. b) Deactivation images of afterglow OLEDs.

order as a result of the long lifetime of the triplet excited states. Although the RTP duration from aromatic molecules is far shorter than that from inorganic system, organic RTP has some advantages, such as easy color tunability, ON/OFF switching ability,[9] and biocompatibility by molecular modification. Further, the presence of triplet absorption can be utilized for reverse saturable absorption [10] and is expected to have applications in nonlinear optics.

Such long-lived RTP (LL-RTP) may be useful for afterglow lighting as an alternative to afterglow fluorescent lamps, which are widely used for residential lighting because they emit a faint glow even after the power supply is switched off. In the case of afterglow OLEDs, long-lived emission can be obtained in the form of electroluminescence (EL) from an organic LL-RTP emitter layer without requiring an extra layer of inorganic phosphor to produce photoluminescence (PL), making such devices attractive for future lighting applications. Furthermore, dual emission of both fluorescence and phosphorescence is another possibility to harvest all singlet and triplet excitons for light emission. Such a system may have advantages over phosphorescent and

TADF emitters, because it can exhibit two different emission colors from a single emitter molecule, leading to white OLEDs with one kind of emitter (**Figure 2-1**).

Effective molecular design guideline for LL-RTP from host–guest systems was investigated by Hirata et al. using hydroxysteroid.[11] The hydroxyl steroid host provides a rigid amorphous environment for guest emitters, which minimizes the nonradiative decay of the long-lived triplet excitons. However, hydroxysteroid is one of the few host matrices shown to suppress all the host-related quenching factors at ambient conditions. While afterglow OLEDs could be realized by introducing an organic LL-RTP emitter layer into an OLED structure, almost all of the LL-RTP host materials reported to date are electrical insulators because their nonaromatic backbones or containing hydroxyl functional groups. Hydrophilic functional groups usually result in electron traps in semiconducting devices.[12] To realize afterglow OLEDs, we need to investigate a wide variety of host matrices to understand the host-related quenching process in more detail.

This chapter presents LL-RTP from aromatic emitters doped into well-known organic semiconducting host materials. I investigated the dependence of the LL-RTP lifetime on the glass transition temperature (T_g), the triplet energy (E_{T1}) of host matrices, and sample temperature. I demonstrate that the triplet energy gap between the emitting materials and the host matrix ($\Delta E_{T1\text{-}T1'}$) plays an important role in LL-RTP. These results are important for the confinement of long-lived triplet excitons in organic semiconducting devices.[13]

2. 2. Results and discussion

2. 2. 1. Dominant factor of k_{nr}^{T} under room temperature

Figure 2-2a shows the aromatic hosts used in this study, most of which are commonly used in OLEDs. The deuterated organic phosphor DMFLTPD-d_{36} (**Fig. 2-2**b) [11] was mixed with these hosts with the concentration of 1 wt% and films were formed using melt casting. The room-temperature phosphorescence decay profiles of these mixed films are shown in **Fig. 2-2**c. The films with β-estradiol, DPEPO, PPT, mCP, and mCBP hosts showed LL-RTP while those with TrisPCz, TPD, and α-NPD hosts showed no LL-RTP. For each doped film, the phosphorescence lifetime ($\tau_{phos}(T)$) was calculated from the first-order exponential fitting of the emission decay profile, and the phosphorescence quantum yield (Φ_{phos}) was calculated from the product of the total emission quantum yield (Φ_{total}) and the ratio of the integrated phosphorescence spectrum to the total integrated emission spectrum (**Table 2-1**).

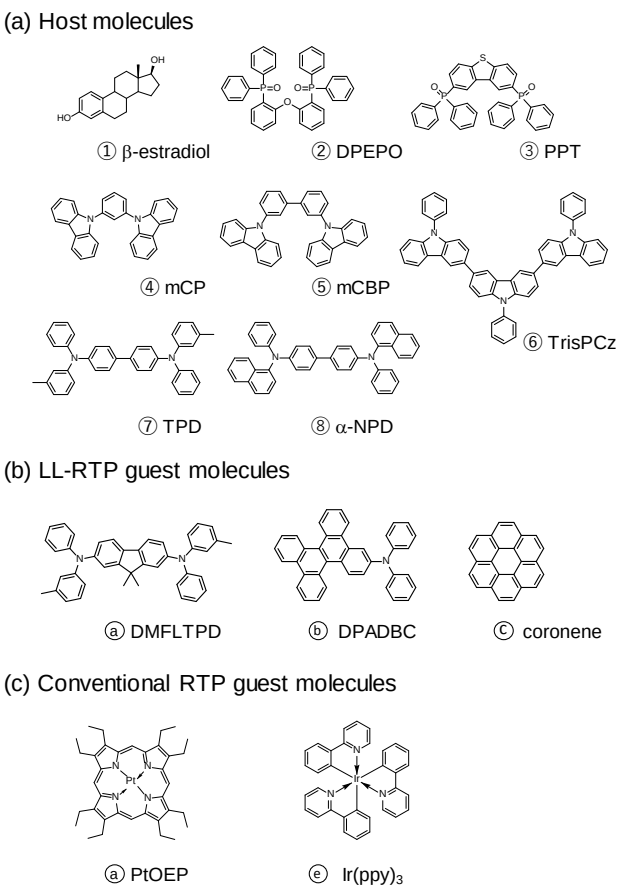

Figure 2-2. a) The molecular structures of hosts, b) LL-RTP guests and c) conventional phosphorescent guests used in this chapter.

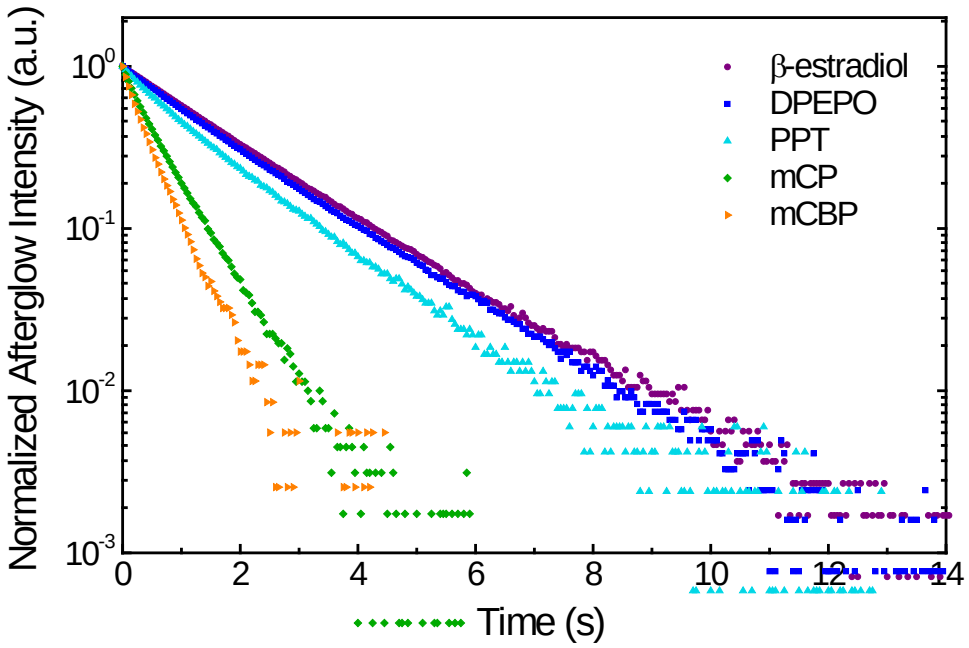

Figure 2-3. Transient room temperature phosphorescence decay curves of DMFLTPD-d_{36} with the dopant concentration of 1 wt% in various host matrices.

Table 2-1. LL-RTP lifetime, triplet energy level, and glass transition temperature of host and guest materials.

	Properties of materials			Properties of doped films				
Property	E_{T1}	$\Delta E_{T1\text{-}T1'}$	T_g	$\tau_{phos}(T)$	Φ_{total}	Φ_{phos}/Φ_{total}	Φ_f	Φ_{phos}
(unit)	eV	eV	K	s	%	%	%	%
DMFLTPD	2.50 [a)]	-	-	-	-	-	-	-
β−estradiol	3.20	0.7	313	1.81	57.4	37.5	35.9	21.5
DPEPO	3.20	0.7	367	1.72	50.0	31.4	34.3	15.7
PPT	2.98	0.48	380	1.50	20.3	68.3	6.4	13.9
mCP	2.85	0.35	339	0.71	41.2	10.3	37.0	4.2
mCBP	2.82	0.32	365	0.45	41.3	10.8	36.9	4.4
TrisPCz	2.65	0.15	427	N. O.[b)]	28.5	0.0	28.5	0.0
TPD	2.40	−0.10	333	N. O. [b)]	35.2	0.0	35.2	0.0
α-NPD	2.30	−0.20	372	N. O. [b)]	24.1	0.0	24.1	0.0

a) measured in frozen 2-MeTHF solution, b) Not observed.

Although the concentration of guest emitter DMFLTPD-d_{36} was constant, the τ_{phos} (T) values varied greatly depending on the host molecules (**Figure 2-3 and Table 2-1**), indicating that the nonradiative decay process is affected by the host molecule. The rate constant of the total nonradiative decay from the triplet excited state (k_{nr}^{T} (T)) can be divided into components from the guest ($k_{nr,guest}^{T}$ (T)) and host ($k_{nr,host}^{T}$ (T)) as follows:[11]

$$k_{nr}^{T}(T) = k_{nr,guest}^{T}(T) + k_{nr,host}^{T}(T). \quad (2\text{-}1)$$

In organic glasses, $k_{nr,host}^{T}$ (T) caused by oxygen quenching was investigated using some emitters, such as $Ir(ppy)_3$, PtOEP, and DMFLTPD-d_{36} (**Fig. 2-2**c), having different k_{phos} from each other. While $Ir(ppy)_3$ showed virtually no changes of the phosphorescent component, PtOEP showed a decrease of Φ_{phos} and $\tau_{phos.}$ (**Figure 2-4** and **Table 2-2**). For DMFLTPD-d_{36}, the phosphorescent emission was disappeared under the air. $k_{nr,host}^{T}$ (T) contributed by oxygen quenching in mCP was confirmed to be 2.6×10^3 s^{-1} through the evaluation of PtOEP doped in an mCP film. Here assumed that Φ of intersystem crossing from S_1 to T_1 (Φ_{isc}) of PtOEP is 100%. Compared with k_{phos} of the LL-RTP emitter, which has less than 10^0 s^{-1}, this value is enough large to quench its phosphorescence.

When aiming to use LL-RTP emitters in OLEDs, the effects of concentration quenching and oxygen quenching can be avoided by using a low concentration of guest molecules and measuring under vacuum conditions. Thus, the main origin of nonradiative decay of triplet excited states is either thermal diffusional motion or reverse energy transfer. To investigate these two factors, I evaluated the thermal and photo-physical properties of the semiconducting host molecules.

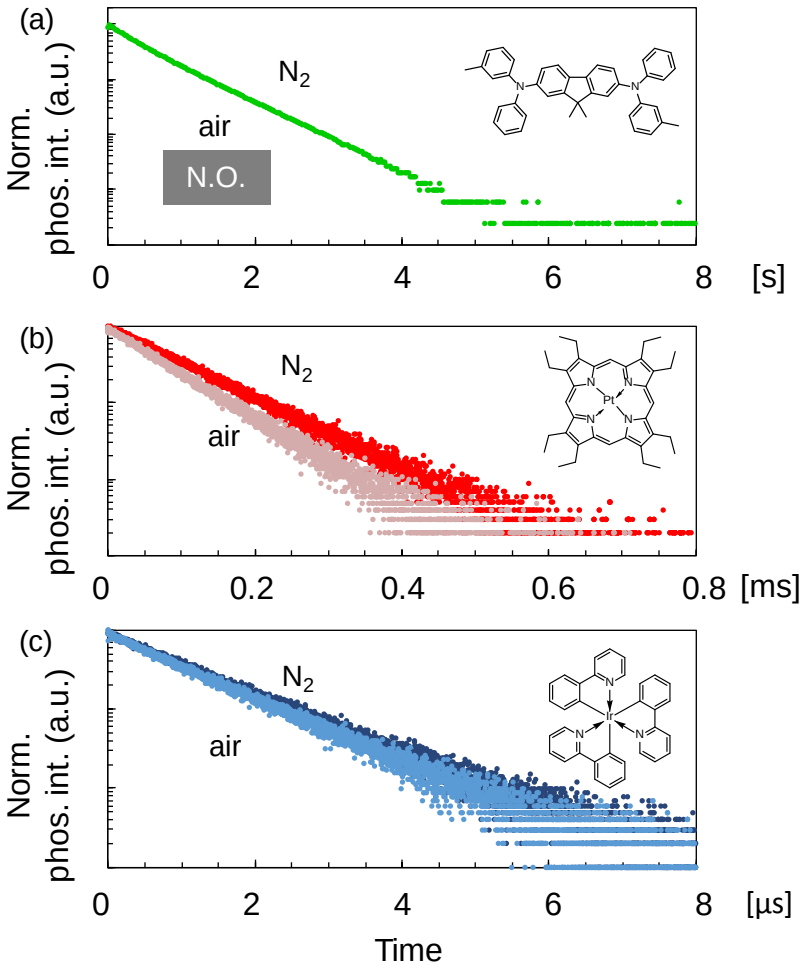

Figure 2-4. Transient phosphorescence decay curves of a) DMFLTPD-d_{36}, b) PtOEP, and c) $Ir(ppy)_3$ doped mCP films in the absence and presence of O_2.

Table 2-2. Phosphorescence lifetime and PLQY of phosphors doped in mCP.

	τ_{phos}		Φ_{phos}	
compound	air	N_2	air	N_2
DMFLTPD-d_{36}	N.O. [b]	0.71 s	N.O. [b]	0.042
PtOEP	72.8 μs	94.2 μs	0.44	0.53
$Ir(ppy)_3$	1.05 μs	1.13 μs	0.90	0.91

b) Not Observed

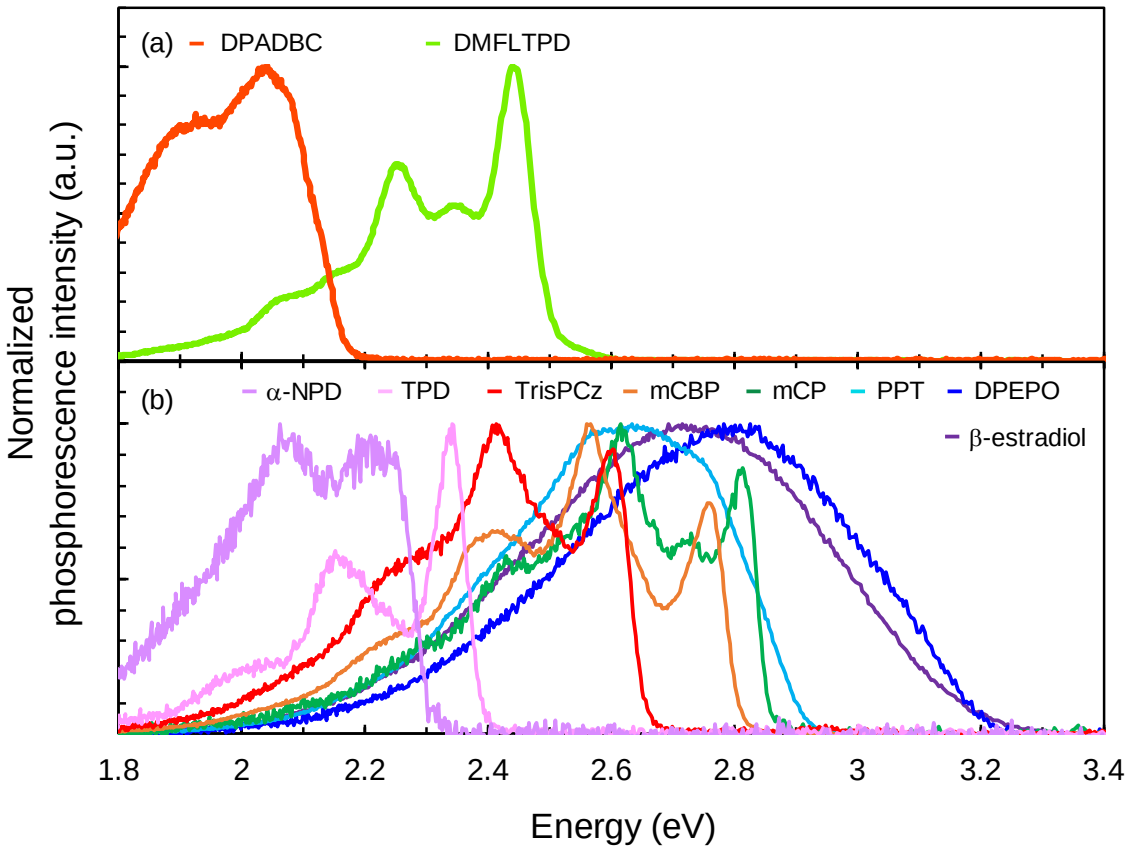

Figure 2-5. Low temperature phosphorescence spectra of a) LL-RTP guests in 2-MeTHF and b) amorphous organic semiconducting hosts formed by melt-cast method.

The glass transition temperature (T_g) of each host was examined using differential scanning calorimetry (DSC) and is shown in **Table 2-1**. All the T_g values are above room temperature, indicating that the hosts can form amorphous films at room temperature. The energy level of the lowest triplet excited state (E_{T1}) of each host was estimated from the onset of the phosphorescence spectrum (**Figure 2-5**) obtained from an amorphous film at 77 K (**Table 2-1**). The phosphorescence spectra of the guest emitter molecules DMFLTPD-d_{36} and deuterated diphenylaminodibenzo[g,p]chrysene (DPADBC-d_{25}), which is discussed later, were obtained from 2-methytetrahydrofuran (2-MeTHF) solution at 77 K.

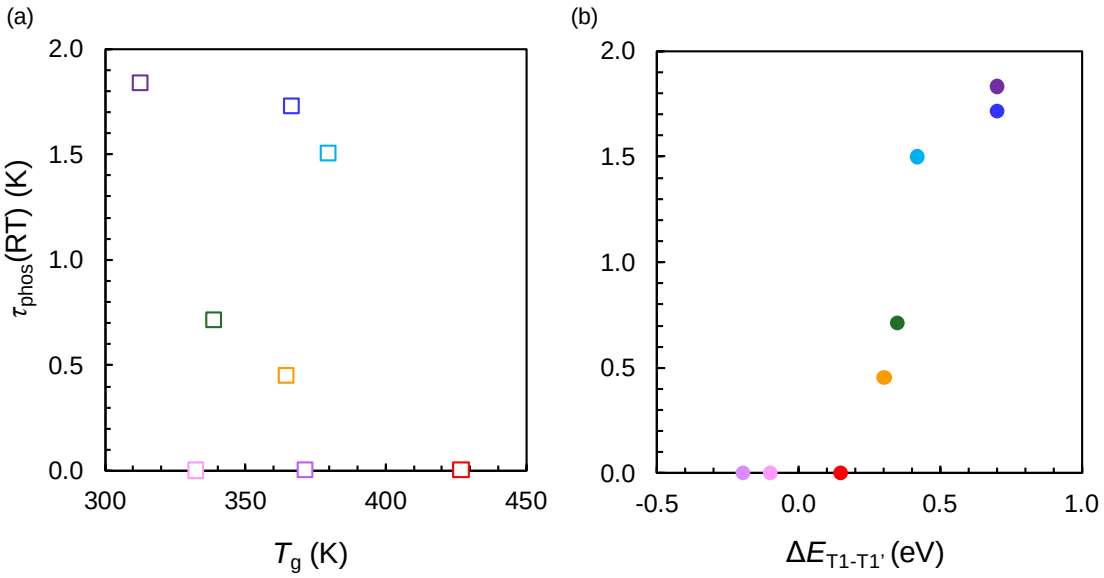

Figure 2-6. The relationship between τ_{phos}(RT) and a) T_g or b) $\Delta E_{T1\text{-}T1'}$ using DMFLTPD-d_{36} doped films.

Based on these results, we could not find a correlation between T_g and τ_{phos}(RT), indicating that the triplet exciton lifetime does not depend on the thermal stability of the organic semiconducting host matrix (**Figure 2-6**a). In contrast, the τ_{phos}(RT) value was strongly dependent on the E_{T1} of host matrix (**Figure 2-6**b). The E_{T1} gaps between host and guest ($\Delta E_{T1\text{-}T1'}$) are summarized in Table 1. Although the E_{T1} gap between mCP (2.85 eV) and DMFLTPD-d_{36} (2.50 eV) would generally be considered sufficient for preventing quenching in OLEDs, the τ_{phos}(RT) was 0.71 s. In the case of DPEPO (3.20 eV), τ_{phos}(RT) increased to 1.72 s. These results indicate that reverse energy transfer from triplet state of guest to host is the main factor for the nonradiative decay of triplet excitons and that a large $\Delta E_{T1\text{-}T1'}$ is required to reduce this process. To confirm this triplet energy transfer process, mixed host matrices of β-estradiol or DPEPO (3.20 eV) and mCBP (2.82 eV) with various concentrations were investigated (**Figure ex2-1**, Appendix). Although τ_{phos}(RT) was almost constant for concentrations of mCBP below 10 wt%, τ_{phos}(RT) drastically decreased for concentrations of mCBP over 10 wt%. This can be explained by

improved Dexter energy transfer from T_1 of the emitter to the T_1 of mCBP because of a shorter distance between them without greatly modifying the matrix rigidity.

The LL-RTP behavior was also examined for vacuum-deposited films to check the dependence of the fabrication process (**Figure 2-7**). Both the amorphous melt-casted glass films and the vacuum-deposited films show almost identical emission decay profiles, indicating that the preparation method has no critical influence.

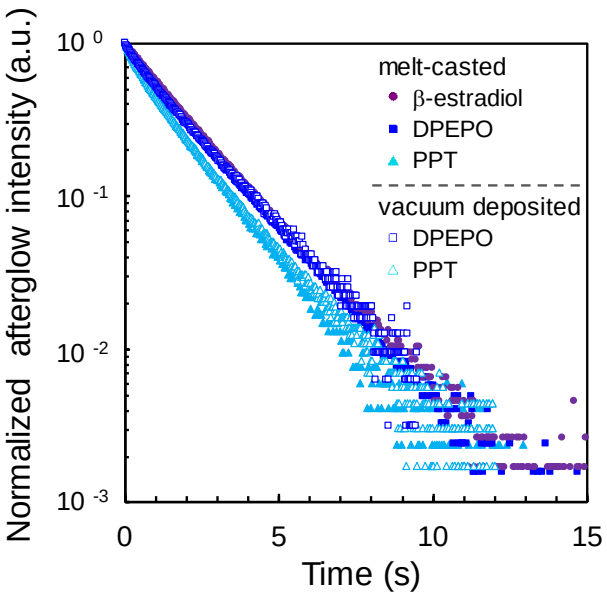

Figure 2-7. Transient phosphorescence decay curves of melt-casted films (closed symbols) and vacuum deposited films (open symbols).

To understand the thermal activation of the reverse energy transfer from guest to host molecules, the phosphorescence decay curves of DMFLTPD-d_{36} doped into β-estradiol, DPEPO, PPT, mCP, mCBP, and TrisPCz glass films were obtained at 5–400 K (**Figure ex2-2**, Appendix). The calculated $\tau_{phos}(T)$ as a function of the reciprocal of temperature are shown in **Figure 2-8**a. The $\tau_{phos}(T)$ values in the low temperature region below 150 K were almost equal for all of the hosts. In contrast, $\tau_{phos}(T)$ rapidly decreased as temperature increased above temperature thresholds that show a correlation with the E_{T1} of the host molecules. The nonradiative deactivation rates ($k_{nr}^{T}(T)$) were calculated from the temperature dependence of $\tau_{phos}(T)$ and are plotted in **Fig. 2-8**b.

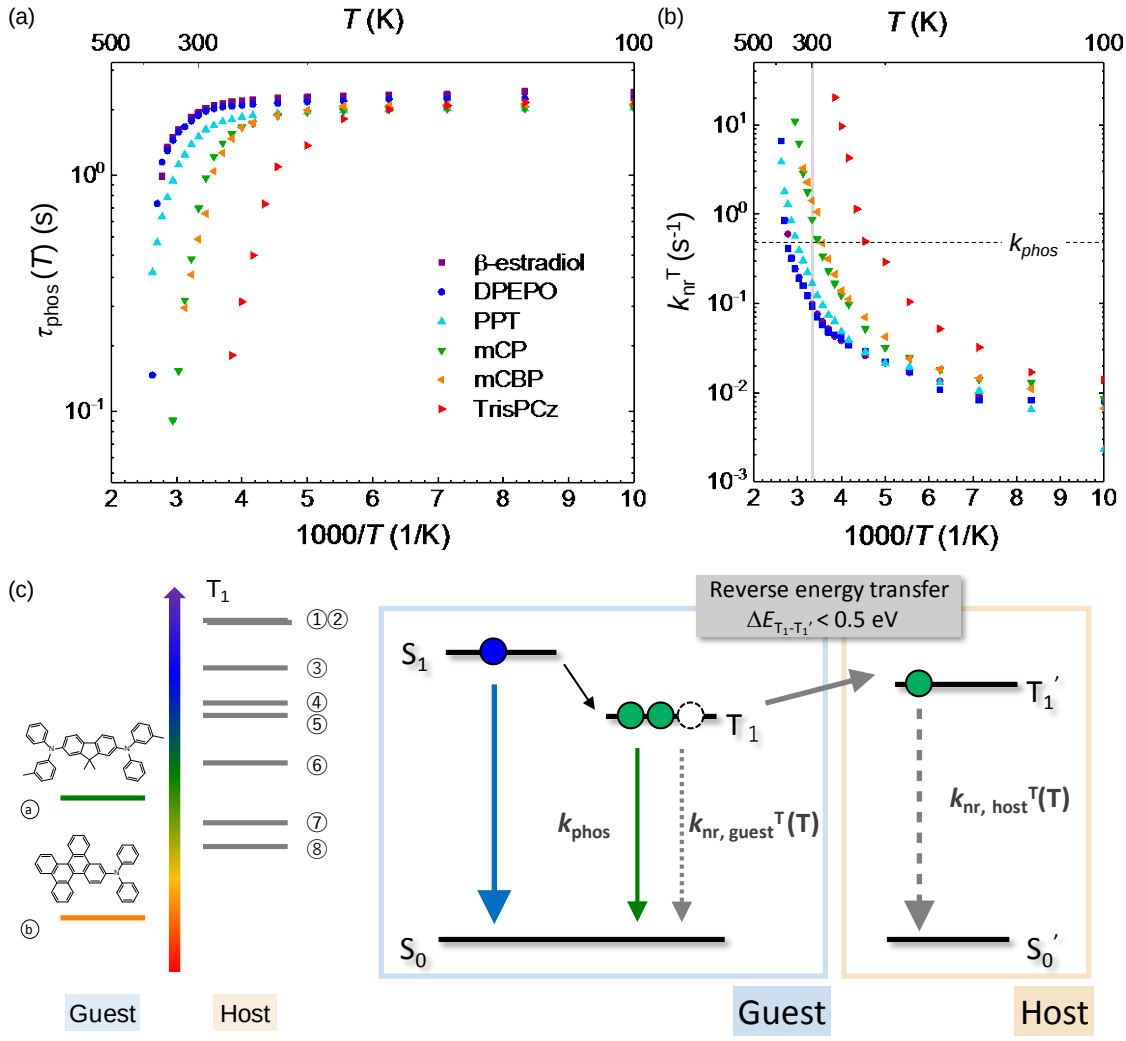

Figure 2-8. a) Temperature dependence of $\tau_{phos}(T)$. b) Temperature dependence of $k_{nr}^{T}(T)$. c) Energy diagram of the materials and the radiative, nonradiative, and energy transfer scheme.

In the low temperature region, all of the host–guest films exhibited a first-order exponential decay of $k_{nr}^{T}(T)$ in the range of 10^{-3} to 10^{-1} s^{-1}. This region can be attributed to the nonradiative deactivation of the guests $k_{nr,guest}^{T}(T)$ because most of the host matrices show similar trends. By increasing temperature, $k_{nr}^{T}(T)$ rapidly increased at certain temperatures that again correlate with the E_{T1} of the host molecules. This increase can be assigned to the nonradiative deactivation of the host $k_{nr,host}^{T}(T)$. Because the k_{nr}(RT) of mCP, mCBP, and TrisPCz were much larger than the k_{phos} of the emitter

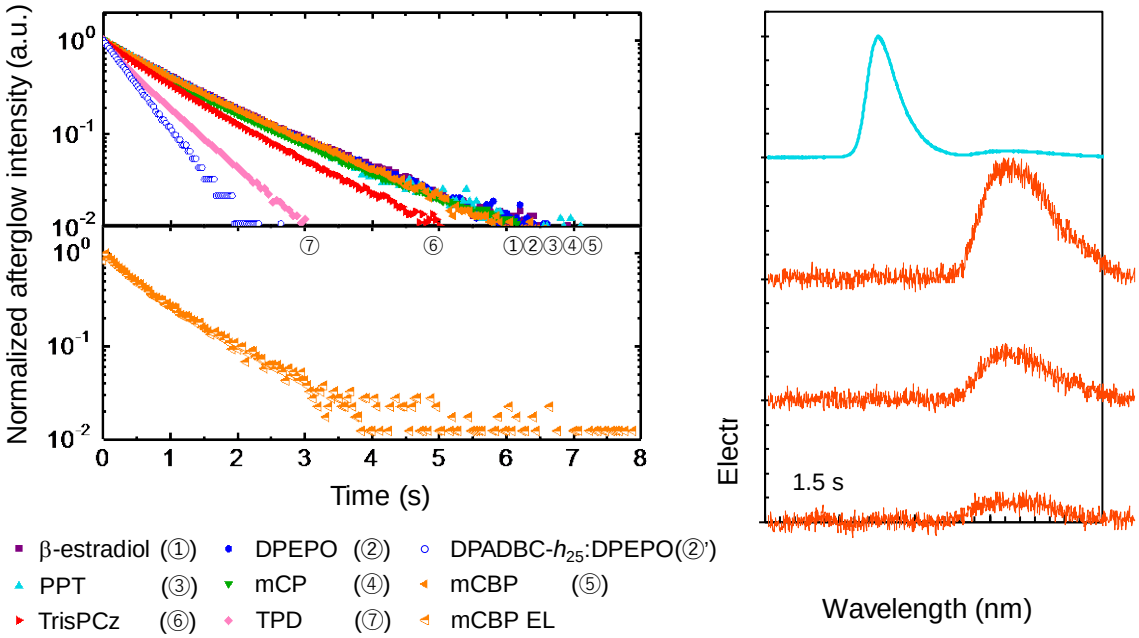

Figure 2-9. Transient decay profiles; a) optically excited, b) electrically excited phosphorescence decay curves and c) EL spectra during (blue) and at different times after (red) excitation of DPADBC-d_{25}.

DMFLTPD-d_{36} (4.8×10^{-1} s^{-1}),[11] the triplet excitons in these host–guest films were deactivated by the host molecules and exhibited a shorter $\tau_{phos}(T)$ at 300 K. Because the $k_{nr,host}^{T}$ (T) value is related not to T_g but the sample temperature, the main deactivation pathway can be ascribed to the thermally assisted reverse energy transfer from the T_1 of the guest to the T_1 of the host (**Fig. 2-8**c). From these results, I conclude that $k_{nr,host}^{T}$ (T) is dominant at room temperature and that a very large $\Delta E_{T1\text{-}T1'}$ of around 0.5 eV is required to confine the long-lived triplet excitons.

To confirm the effect of $\Delta E_{T1\text{-}T1'}$ on LL-RTP, I also investigated a lower E_{T1} emitter of deuterated LL-RTP emitter (DPADBC-d_{25}) [9b,11] (**Fig. 2-2**b). The E_{T1} for DPADBC-d_{25} of 2.20 eV obtained from the phosphorescence spectrum in 2-MeTHF solution at 77 K is much lower than that of 2.50 eV for DMFLTPD-d_{36} (**Fig. 2-5**). This lower E_{T1} value of the emitter results in a large $\Delta E_{T1\text{-}T1'}$ when paired with most of the host molecules. **Figure 2-9**a shows the emission decay curves of DPADBC-d_{25} doped into fil

ms of each of the host molecules. Although the τ_{phos}(RT) of 1.25 s in β-estradiol is slightly shorter than the reported value [11] due to the incomplete deuteration (Figure S5), the films with β-estradiol, DPEPO, PPT, mCP, and mCBP as host showed almost identical emission decay profiles at room temperature (**Figure 2-10**). These results indicate the contribution of $k_{nr,host}^{T}$ (RT) in these hosts is sufficiently small because of a large $\Delta E_{T1\text{-}T1'}$ of over 0.6 eV. The $\tau_{phos}(T)$ values decreased with decreasing $\Delta E_{T1\text{-}T1'}$ in the hosts of TrisPCz, TPD, and α-NPD. Thus, a very large $\Delta E_{T1\text{-}T1'}$ of around 0.5 eV is essential to prevent the reverse energy transfer of long-lived triplet excitons from guest to host. This required $\Delta E_{T1\text{-}T1'}$ values are much larger than the conventional host–guest energy gap of 0.1–0.2 eV used in conventional OLEDs.[14] Based on the Boltzmann statistics, the energy gap of 0.5 eV corresponds to a significant difference of two states' population of ~10^9. Thus, vibrational coupling between guest and host molecules and the local fluctuation of their molecular energy during very long triplet lifetime would enable the guest to host energy transfer.

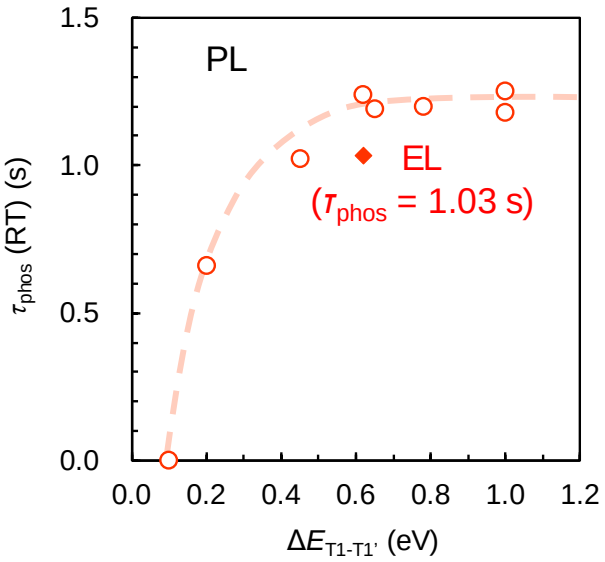

Figure 2-10. Relationship between τ_{phos}(RT) and $\Delta E_{T1\text{-}T1'}$ using DPADBC-d_{25} and the hosts.

Furthermore, the experimental data between τ_{phos}(RT) and $\Delta E_{T1\text{-}T1'}$ using DMFLTPD-d_{36} and DPADBC-d_{25} as the guest were compared with the equation (2-2, 3). Here, $k_{nr,host}^{T}$(RT) was assumed to be based on an Arrhenius equation considering Boltzmann distribution.

$$\tau_{phos}(T) = 1/ (k_{phos} + k_{nr,guest}^{T}(T) + k_{nr,host}^{T}(T)) , \quad (2\text{-}2)$$

$$k_{nr,host}^{T}(T) = A \times \exp(-\Delta E_{T1\text{-}T1'} /k_B T) . \quad (2\text{-}3)$$

($k_{phos} + k_{nr,guest}^{T}$(RT)) was presumed by the reciprocal value of τ_{phos}(RT) using β-estradiol as the host. Each plot did not match with any *A* value (**Figure ex2-3**, Appendix). To deepen understanding the mechanism of reverse energy transfer from guest to host, more precise models incorporating the effect of the nonradiative deactivation from T_1 to S_0 of host matrices or the cycle of forward and reverse energy transfer between host matrices and guest emitters should be considered.

Because of most of the semiconducting host–guest films exhibited LL-RTP, we examined their operation under electrical excitation with the aim of achieving afterglow OLEDs. In case of DMFLTPD-d_{36}, optimization of an OLED with the hosts used here is difficult because of the high E_{T1} needed for the surrounding layers, so only DPADBC-d_{25} was considered. An OLED containing DPADBC-d_{25} doped in mCBP as the active layer was fabricated by vapor deposition and operated by applying short voltage pulses of 50 μs. The structure of the OLED was composed of the multi-layers of ITO (100 nm), TrisPCz (30 nm), mCBP (10 nm), 1 wt% DPADBC-d_{25}: mCBP (30 nm), PPT (40nm), LiF (0.8nm), and Al (100 nm). Although the OLED exhibited green emission mainly derived from fluorescence of DPADBC-d_{25} during pulse duration, I obtained orange afterglow emission attributed to the phosphorescence of DPADBC-d_{25} when the applied voltage was turned off (**Fig. 2-9**c). The transient electroluminescence decay curve shown in **Fig. 2-9**b was almost identical to the photoluminescence decay curve of DPADBC-d_{25} doped in mCBP because of the small contribution of $k_{nr,host}^{T}$ (RT) derived from the large $\Delta E_{T1\text{-}T1'}$. Although triplet energy confinement is very important for harvesting the triplet excitons as emission, our results indicate that the required $\Delta E_{T1\text{-}T1'}$ value depends on the

lifetime of the triplet excitons. A conventional $\Delta E_{T1\text{-}T1'}$ of 0.1–0.2 eV is enough for emitters having short triplet lifetime but would be not sufficient for some triplet-related emitters having longer triplet lifetimes, such as emitters utilizing long-lived phosphorescence or thermally activated delayed fluorescence (TADF).

2. 2. 2. Maximization of triplet exciton lifetime of guest molecule

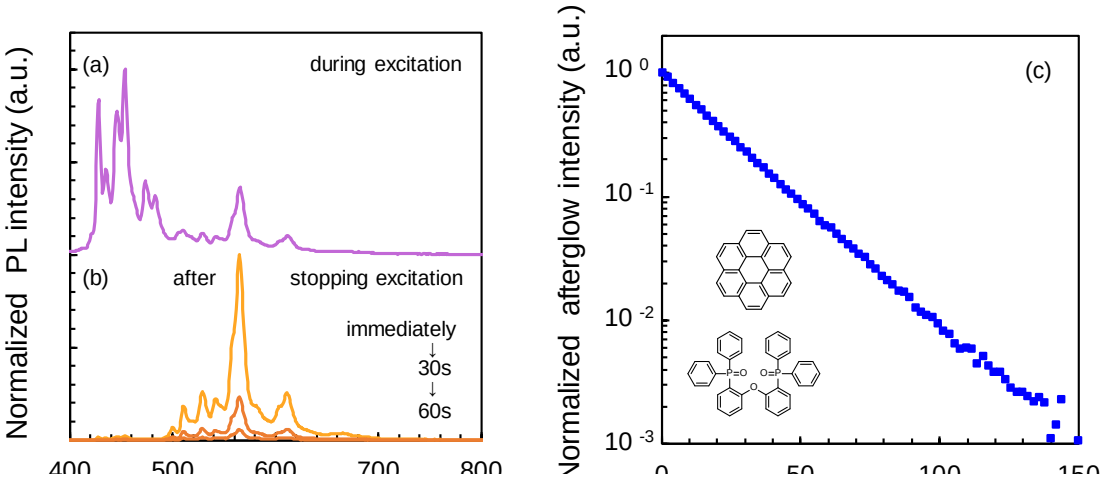

Figure 2-11. The photoluminescence profiles of film; the PL spectra a) during excitation and b) after stopping excitation, and c) decay curve after stopping excitation.

To maximize τ_{phos} of afterglow emission, deuterated coronene-d_{12} (E_{T1} = 2.46 eV, **Figure ex2-4**, Appendix) was introduced as an emitter, which exhibited LL-RTP of over 20 s doped in a polymethylmethacrylate film.[15] Coronene-d_{12} was obtained by deuteration of coronene-h_{12} in mixture solvent comprising D_2O, cyclohexane and 2-propanol under an ordinary atmosphere. **Figure 2-11** presents the PL profiles of coronene- d_{12} doped in a DPEPO film at a concentration of 1wt% at room temperature. Because of the highly symmetrical (D_{6h}) chemical structure and pure π-π* transition of coronene-d_{12}, the phosphorescence decay constant was minimized, and it exhibited sharp fluorescence and phosphorescence. A long τ_{phos}(RT) of 21.1 s was observed with coronene-d_{12} doped in a DPEPO. k_{nr}^{T}(RT) = 7.6×10^{-3} s^{-1} and k_{phos} = 4.0×10^{-2} s^{-1} was obtained from temperature

dependent PL measurement because of the small k_{phos} and $k_{nr,guest}^{T}$ originated from coronene-d_{12} and $k_{nr,host}^{T}$ by securing enough $\Delta E_{T1\text{-}T1'}$. Φ_{phos} was calculated to be 12.7% from Φ_{total} of 39.7%. This host-guest pair can be installed to emitting layer of OLEDs to achieve effective afterglow emission.

2. 3. Conclusion

In conclusion, I demonstrated that many conventional organic semiconducting host–guest systems exhibit LL-RTP under optical and electrical excitation. I confirmed that the main deactivation pathway of the long-lived triplet excitons under absence of molecular oxygen is the reverse energy transfer from guest emitter to host molecule by comparing the E_{T1} and T_g of the hosts and the radiative and nonradiative rate constants. To minimize reverse energy transfer, long-lived excitons ($k_{phos} < 10^0$ s^{-1}) require a very large triplet energy gap $\Delta E_{T1\text{-}T1'}$ of around 0.5 eV, which is a much larger value than in conventional host–guest systems. Our results indicate that $\Delta E_{T1\text{-}T1'}$ needs to be considered when the emitters have long triplet exciton lifetimes, such as in the cases of long-lived phosphorescence.

2. 4. Experimental methods

2. 4. 1. Preparation of samples

The compounds DMFLTPD-d_{36}, DPADBC-d_{25},[11] PPT,[16] and DPEPO [17] were prepared as described in the literature while α-NPD, TPD, TrisPCz, mCBP, and mCP were obtained commercially and purified by sublimation.

Deuteration of aromatic hydrocarbons

Coronene-h_{12} 500mg, 3wt% Pt/C 200mg, deuterium oxide 20mL, 2-propanol 1mL

and cyclohexane 9mL were heated at 80 ℃ for 24 h. This reaction was repeated several times until hydrogen of coronene was substituted for deuterium. After cooling, coronene was extracted with toluene and filtered through celite®. After organic solvent was reduced by evaporation, recrystallized and then filtered. The deuteration ratio was 95.8%.

Deuteration ratio was calculated from NMR spectra by using 1,4-dioxane as an internal standard.

Glass samples were prepared by heating powders of the materials above the melting point of the host materials on silicon or quartz substrates under nitrogen atmosphere and then cooling down the samples to room temperature immediately. Guest molecules were mixed with each host in a concentration of 1 wt% before annealing. Vacuum-deposited films were fabricated on quartz substrates by thermal evaporation at a pressure lower than 1×10^{-3} Pa.

An OLED was fabricated on an indium tin oxide (ITO) patterned glass substrate by thermal evaporation at a pressure lower than 7×10^{-4} Pa. The device was encapsulated in a nitrogen atmosphere using UV-cured epoxy resin and a glass cover.

2. 4. 2. Characterization of properties of samples

T_g was examined by DSC (204 F1 Phoenix, Netzsch) under N_2.

The temperature dependence of the transient photoluminescence characteristics was measured using a photomultiplier tube and a multichannel analyzer (PMA-12, Hamamatsu Photonics) under vacuum conditions. Samples were excited at 325 nm with a He-Cd laser.

The Φ_{total} was measured using an absolute PL quantum yield measurement system (Quantaurus-QY C11347-01, Hamamatsu Photonics) under argon gas flow with an

excitation wavelength of 325 nm. The fluorescence quantum yields (Φ_{flu}) and phosphorescence quantum yields (Φ_{phos}) were determined from the emission spectra and Φ_{total} as described in the literature.[11]

$$\Phi_{total} = \Phi_{flu} + \Phi_{phos} . \quad (2\text{-}4)$$

The phosphorescence efficiencies of OLEDs were also determined by same method.

The total value of $k_{nr}^{T}(T)$ at each temperature was calculated using [11]

$$k_{nr}^{T}(T) = 1/\tau_{phos}(T) - k_{phos} . \quad (2\text{-}5)$$

Because the nonradiative decay of guest molecules at 5 K is presumed to be 0:

$$k_{nr}^{T}(5\ K) = 0 , \quad (2\text{-}6)$$

k_{phos} was calculated using

$$k_{phos} = 1/\tau_{phos}(5\ K) . \quad (2\text{-}7)$$

External quantum efficiency (η_{EQE}) – current density (J) and J – voltage (V) characteristics were measured using a Keithley 2400 source meter and external quantum efficiency measurement system (C9920-12, Hamamatsu Photonics). Transient electroluminescence characteristics were measured using a photomultiplier tube and PMA-12. The applied voltage was adjusted to 250 mA cm^{-2}.

2. 5. References

[1] a) F. Liu, W. Yan, YJ. Chuang, Z. Zhen, J. Xie, Z. Pan, *Sci. Rep.* **2013**, *3*, 1554; b) Z. Pan, Y-Y. Lu, F. Liu, *Nat. Mater.* **2012**, *11*, 53.

[2] T. Matsuzawa, Y. Aoki, N. Takeuchi, Y. Murayama, *J. Electrochem. Soc.* **1996**, *143*, 2670.

[3] a) G. Oster, N. Geacintov, A. U. Khan, *Nature* **1962**, *196*, 1089; b) H. A. Al-Attar, A. P. Monkman, *Adv. Funct. Mater*. **2012**, *22*, 3824; c) S. Reineke, M. A. Baldo, *Sci. Rep.* **2014**, 4, 3797; d) S. Reineke, N. Seidler, S. R. Yost, F. Prins, W. A. Tisdale, M. A. Baldo, *Appl. Phys. Lett.* **2013**, *103*, 093302.

[4] a) S. Scypinski, L. J. C. Love, *Anal. Chem.* **1984**, *56*, 322; b) S. Scypinski, L. J. C. Love, *Anal. Chem.* **1984**, *56*, 331.

[5] a) C. Li, X. Tang, L. Zhang, C. Li, Z. Liu, Z. Bo, Y. Q. Dong, Y.-H. Tian, Y. Dong, B. Z. Tang, *Adv. Opt. Mater.* **2015**, *3*, 1184; b) Y. Gong, G. Chen, Q. Peng, W. Z. Yuan, Y. Xie, S. Li, Y. Zhang, and B. Z. Tang, *Adv. Opt. Mater.* **2015**, *27*, 6195; c) J. Wei, B. Liang, R. Duan, Z. Cheng, C. Li, T. Zhou, Y Yi, Y. Wang, *Angew. Chem. Int. Ed.* **2016**, *55*,15589.

[6] Z. An, C. Zheng, Y. Tao, R. Chen, H. Shi, T. Chen, Z. Wang, H. Li, R. Deng, X. Liu, W. Huang, *Nat. Mater.* **2015**, *14*, 685.

[7] X. Yang, D. Yan, *Adv. Opt. Mater.* **2016**, *6*, 897.

[8] H. Mieno, R. Kabe, N. Notsuka, M. D. Allendorf, C. Adachi, *Adv. Opt. Mater.* **2016**, *4*, 1015.

[9] a) S. Hirata, K. Totani, H. Kaji, M. Vacha, T. Watanabe, C. Adachi, *Adv. Opt. Mater.* **2013**, *1*, 438; b) Y. Katsurada, S. Hirata, K. Totani, T. Watanabe, M. Vacha, *Adv. Opt. Mater.* **2015**, *3*, 1726.

[10] S. Hirata, K. Totani, T. Yamashita, C. Adachi, M. Vacha, *Nat. Mater.* **2014**, *13*, 938.

[11] S. Hirata, K. Totani, J. Zhang, T. Yamashita, H. Kaji, S. R. Marder, T. Watanabe, C. Adachi, *Adv. Funct. Mater.* **2013**, *23*, 3386.

[12] L. L. Chua, J. Zaumseil, J. F. Chang, E. C.-W. Ou, P. K.-H. Ho, H. Sirringhaus, R. H. Friend, *Nature* **2005**, *434*, 194.

[13] a) Q. Wanga, H. Aziz, *Appl. Phys. Lett.* **2014**, *105*, 053304; b) R. Kabe, N. Notsuka, K. Yoshida, C. Adachi, *Adv. Mater.* **2016**, *28*, 655.

[14] a) R. J. Holmes, B. W. D'Andrade, S. R. Forrest, X. Ren, J. Li, M. E. Thompson, *Appl. Phys. Lett.* **2003** *83*, 3818; b) M. A. Baldo, S. R. Forrest, *Phys. Rev. B* **2000**, *62*, 10958; c) F. C. Chen, G. F. He, Y. Yang, *Appl. Phys. Lett.* **2003**, *82*, 1006; d) K. Goushi, R. Kwong, J. J. Brown, H. Sasabe, C. Adachi, *J. Appl. Phys.* **2004**, *95*, 7798.

[15] J. L. Kropp, W. R. Dawson, *J. Phys. Chem.* **1967**, 71, 4499.

[16] S. H. Jeong, J. Y. Le, *J. Mater. Chem.* **2011**, *21*, 14604.

[17] C. Han, Y. Zhao, H. Xu, J. Chen, Z. Deng, D. Ma, Q. Li, P. Yan, *Chem. Eur. J.* **2011**, *17*, 5800. Tang, C. W.; S. A. VanSlyke, S. A. Organic electroluminescent diodes.

Appl. Phys. Lett. **1987**, *51*, 913-915.

Chapter 3

Observation of Nonradiative Deactivation Behavior from Singlet and Triplet States of Thermally Activated Delayed Fluorescence Emitters in Solution

"Observation of Nonradiative Deactivation Behavior from Singlet and Triplet States of Thermally Activated Delayed Fluorescence Emitters in Solution"
Naoto Notsuka, Hajime Nakanotani, Hiroki Noda, Kenichi Goushi, Chihaya Adachi.
Journal of Physical Chemistry Letters DOI: 10.1021/acs.jpclett.9b03302.

3. 1. Introduction of Chapter 3

Organic molecules exhibiting thermally activated delayed fluorescence (TADF) have been one of the important research fields to understand the exciton dynamics.[1-5] Because bright singlet excitons in purely organic molecules exhibiting TADF can access dark triplet excited-states, generated excitons can decay nonradiatively through both singlet and triplet excited-states. Excited states of emissive organic molecules undergo various kinds of quenching phenomena such as vibration-coupled quenching depending on their environmental conditions. Simultaneous suppression of k_{nr} and acceleration of k_{risc} is required to realize nearly 100% yield for triplet harvesting in delayed fluorescence. Thus, investigation of nonradiative decay behavior in TADF emitters is worthwhile.

When the transient PL signals of TADF materials are measured, a second exponential decay component can be observed unlike with fluorescent or phosphorescent materials. The prompt component is a direct radiative transition from the lowest excited singlet state (S_1) to S_0 after photoexcitation. This emission is related to the radiative decay rate constant of fluorescence (k_{flu}) and generally has a high intensity because of its spin-allowed transition. The delayed component is related to k_{risc} and has weaker and longer emission decay characteristics than those of fluorescence because of endothermic and spin-flip processes from the lowest excited triplet state (T_1) to S_1. The delayed component intensity and lifetime strongly depend on k_{risc} because the radiative decay rate constant for the delayed component (k_{delay}) can be described as $k_{delay} = k_{risc} \times (1 - (k_{isc} / (k_{flu} + k_{nr}^{S} + k_{isc})) + k_{nr}^{T}$. To calculate the rate constants of TADF materials from these characteristic PL signals,[6-8] it is necessary to separate the total quantum yield into prompt and delayed components.[9-10] Acquiring two curves, i.e., prompt and delayed emission profiles, requires high-performance measurement systems with wide dynamic ranges of five or six

orders of magnitude for emission intensity and a nanosecond to a second for time scales. One approach to estimate accurate prompt fluorescence/delayed fluorescence ratios requires separate measurements for data on the different time scales.[11-12] Clarification of nonradiative deactivation processes from singlet and triplet states separately can be helpful to comprehensively determine all decay processes.

In this chapter, I investigated the activation and deactivation behaviors of typical TADF molecules under different purged conditions to understand the nonradiative decay channels. By analyzing the PL profiles, I observed oxygen quenching from both S_1 and T_1 of TADF in solution. To understand the oxygen quenching effect, I calculated a prompt fluorescence/delayed fluorescence ratio, even in TADF materials with very different time scales, and the emission intensities of the prompt and delayed components. I also compared the PL performances with those reported previously [5] and identified the nonradiative deactivation behaviors.

3. 2. Result and discussion

To assess the radiative and nonradiative deactivation processes of various TADF molecules, phthalonitrile- (PN) and triphenyl triazine-based molecules were selected as model compounds and their optical properties were measured.[5,13-14] **Figure 3-1** shows the TADF molecules used in this

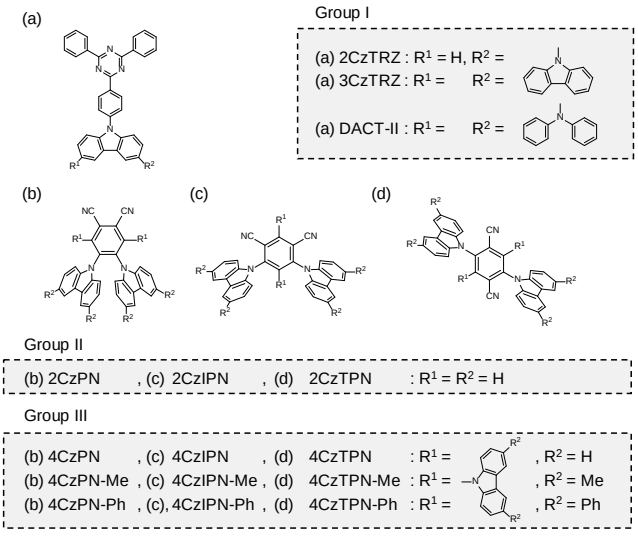

Figure 3-1. Molecular structures of the TADF materials used in this chapter.

study. In a non-polar solvent such as toluene with a dilute concentration condition, a degradation of molecules resulted from an ionization or a radical formation is poorly occurred. Thus, photo-activation and -deactivation processes were considered to proceed cyclically.

3. 2. 1. Bimolecular exciton quenching

For each TADF molecule, lengthening decay lifetimes at the characteristic prompt and delayed components and enhancement of the PL quantum yield (PLQY) were observed with a change from an air- to N_2-saturated solution (**Table 3-1**).

Table 3-1. Photo physical properties of TADF materials in toluene solution.

compounds	$\tau_{prompt,air}$	$\tau_{prompt,N2}$	$\tau_{delay,air}$	$\tau_{delay,N2}$	k_{flu}	$k_{nr,int}^{T}$	k_{isc}	k_{risc}	$k_{q,O2}^{S}$	$k_{q,O2}^{T}$
	ns	ns	μs	μs	10^7 s^{-1}	10^5 s^{-1}	10^7 s^{-1}	10^5 s^{-1}	10^7 s^{-1}	10^6 s^{-1}
2CzTRZ	6.58	8.47	N.O. [a)]	87.9	9.89	0.08	1.91	0.04	3.41	-
3CzTRZ	6.12	7.58	N.O. [a)]	64.2	11.2	0.12	2.02	0.05	3.15	-
DACT-II	8.79	12.7	N.O. [a)]	5.42	4.82	1.48	3.06	0.60	3.49	-
2CzPN	15.2	25.8	N.O. [a)]	177	1.37	0.05	2.50	0.03	2.69	-
2CzIPN	6.98	8.79	N.O. [a)]	111	1.96	0.03	9.41	0.33	2.94	-
2CzTPN	15.4	23	N.O. [a)]	179	2.26	0.03	2.07	0.04	2.15	-
4CzPN	9.41	11	0.348	13.8	1.19	0.09	7.89	4.82	1.55	2.80
4CzPN-Me	10.1	11.9	0.301	5.67	0.96	0.82	7.47	8.28	1.47	3.15
4CzPN-Ph	10.9	12.5	0.322	2.28	1.15	1.95	6.88	17.0	1.11	2.67
4CzIPN	11.5	14.6	0.347	4.57	1.52	0.12	5.32	9.29	1.87	2.67
4CzIPN-Me	10.7	13.2	0.286	2.66	1.74	0.62	5.86	13.7	1.71	3.13
4CzIPN-Ph	16.6	22	0.315	1.6	1.74	2.13	2.82	10.8	1.45	2.55
4CzTPN	6.17	6.6	0.612	2.59	2.92	0.55	12.2	17.2	1.05	1.25
4CzTPN-Me	5.85	6.4	0.299	1.61	2.49	3.81	13.1	15.1	1.47	2.72
4CzTPN-Ph	8.43	9.53	0.254	0.772	1.82	12.2	8.68	4.34	1.36	2.65

a) Not observed.

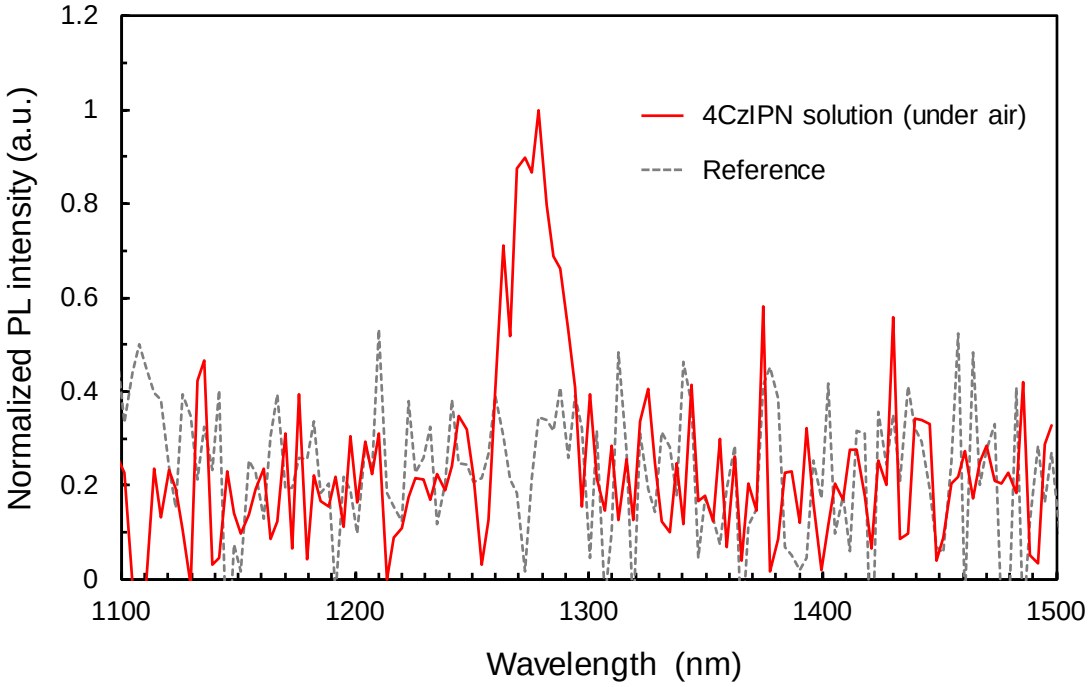

Figure 3-2. Phosphorescence spectrum of $O_2(^1\Delta_g)$ using 4CzIPN as a singlet oxygen photosensitizer.

As in our previous study,[5] 4CzIPN showed a dramatic increase in the delayed component upon removal of dissolved molecular oxygen (O_2) from the solution. Furthermore, to evidently confirm the quenching of the triplets of the TADF molecule by O_2, spectroscopic measurement of excited singlet oxygen, $O_2(^1\Delta_g)$, using 4CzIPN as a photosensitizer was performed under the air atmosphere (**Figure 3-2**). The emission with the peak around 1270 nm supports that photogenerated singlet excitons accessed to triplet and quenched them in the presence of O_2.[15] However, slight increases in the prompt components were also observed in all solutions. **Figure 3-3** shows the PL decay profiles of 4CzIPN and DACT-II, which had remarkably different decay behaviors. Here, I determined the intrinsic PL quantum yield (PLQY) under a degassed condition of a prompt component ($\Phi_{prompt,N2}$) from the product of $\Phi_{prompt,air}$ multiplied by the emission

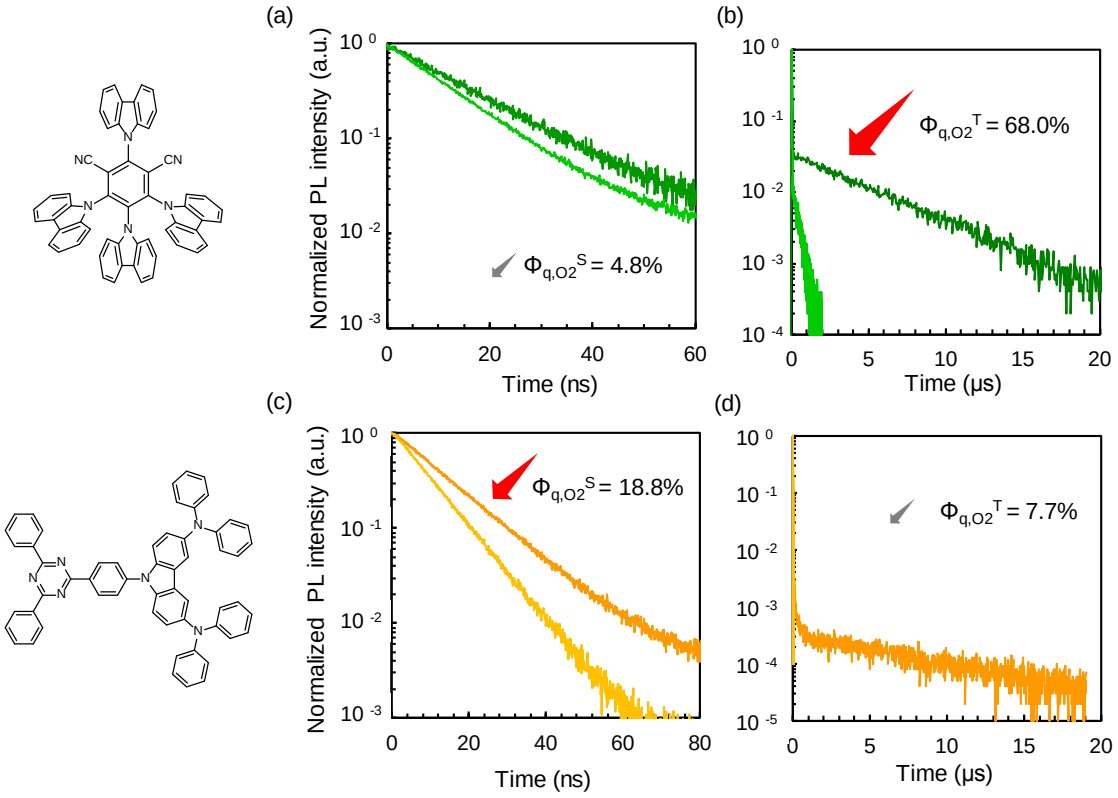

Figure 3-3. Decay curves of a) the prompt component, and b) the delayed components of 4CzIPN and c), d) DACT-II before and after purging with inert gas.

decay lifetime ratio of the prompt components under degassed and air-saturated conditions ($\tau_{prompt,N2}/\tau_{prompt,air}$). The PLQY of the delayed component (Φ_{delay}) was determined by subtracting $\Phi_{prompt,\ N2}$ from the total PLQY. The τ_{prompt} of 4CzIPN changed slightly from 11.5 ns to 14.6 ns when the solution was degassed. The decrease in PLQY with O_2 ($\Delta\Phi_{q,O2}$) was 72.8%, which was made up of 4.8% of singlet quenching ($\Delta\Phi_{q,O2}{}^S$) and 68.0% of triplet quenching ($\Delta\Phi_{q,O2}{}^T$). For DACT-II, τ_{prompt} increased from 8.9 ns to 12.7 ns upon degassing and the $\Delta\Phi_{q,O2}$ of 26.5% was made up of 18.8% of $\Delta\Phi_{q,O2}{}^S$ and 7.7% of $\Delta\Phi_{q,O2}{}^T$. Interestingly, $\Delta\Phi_{q,O2}{}^S$ was greater than $\Delta\Phi_{q,O2}{}^T$ in this case. A previous study focused on oxygen quenching from S_1 for 3CzTRZ.[16] The 3CzTRZ in toluene showed no delayed fluorescence and a fingerprint for population of the triplet state was not observed at room temperature. The missing triplet feature could be attributed to k_{flu}

being four orders of magnitude larger than k_{risc}. In our measurements, delayed fluorescence was observed with τ_{delay} = 64.2 μs and Φ_{delay} = 3.8% (**Figure 3-4**).

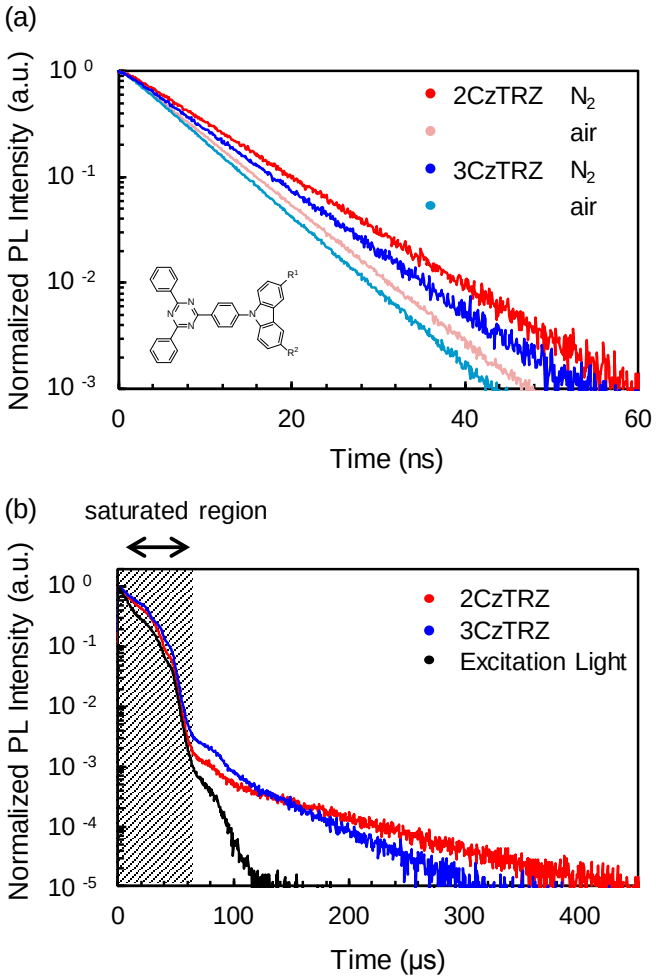

Figure 3-4. a) Prompt and b) delayed transient PL decay profiles of 2CzTRZ and 3CzTRZ excited by flash lamp.

Figure 3-5a and **Table 3-2** summarize the deactivation processes from both S_1 and T_1 in each TADF material. Strong oxygen quenching in the prompt component was observed for the compounds in group I (**Fig. 3-1**), whereas strong quenching was observed for the delayed component in the group III compounds. Thus, some singlet excitons are definitely quenched by O_2. Previously, oxygen quenching in many TADF materials has only been discussed for triplets because of their long lifetimes. Here we note the linearity of the rate constant of oxygen quenching from S_1 and T_1 ($k_{q,O2}^{S,T}$) for the partial pressure of O_2. Both $k_{q,O2}^{S}$ and $k_{q,O2}^{T}$ increase proportionally to the partial pressure of O_2 from the atmospheric oxygen concentration to 100%, respectively (**Table 3-1, 3-2** and **Figure ex3-1,** Appendix). Such quenching behavior of singlet excitons by O_2 could be explained by formation of a contact charge-transfer (CCT) state between an excited molecule and O_2, which could occur via several

processes:[17-22]

Table 3-2. Decay lifetimes of TADF materials in toluene after purging with O_2.

compound	$\tau_{prompt,O2}$ (ns)	$\tau_{delay,O2}$ (μs)
SHT02	3.43	N.O. [a]
DACT-II	3.98	N.O. [a]
2CzPN	5.98	N.O. [a]
4CzIPN	6.28	0.08

a) Not Observed

Table 3-3. Oxygen quenching rate constants of TADF materials in toluene.

	air-saturated [b]		O_2-Purged [c]		Ratio	
compound	$k_{q,O2}^S$ (s^{-1})	$k_{q,O2}^T$ (s^{-1})	$k_{q,O2}^S$ (s^{-1})	$k_{q,O2}^T$ (s^{-1})	$k_{q,O2}^S$ (air/O_2)(%)	$k_{q,O2}^T$ (air/O_2)(%)
SHT02	3.15×10^7	-	1.60×10^8	-	21.0	-
DACT-II	3.49×10^7	-	1.72×10^8	-	20.6	-
2CzPN	2.69×10^7	-	1.28×10^8	-	19.7	-
4CzIPN	1.87×10^7	2.67×10^6	9.09×10^7	1.18×10^7	20.2	22.6

b) under air-saturated condition. c) under O_2-purged condition.

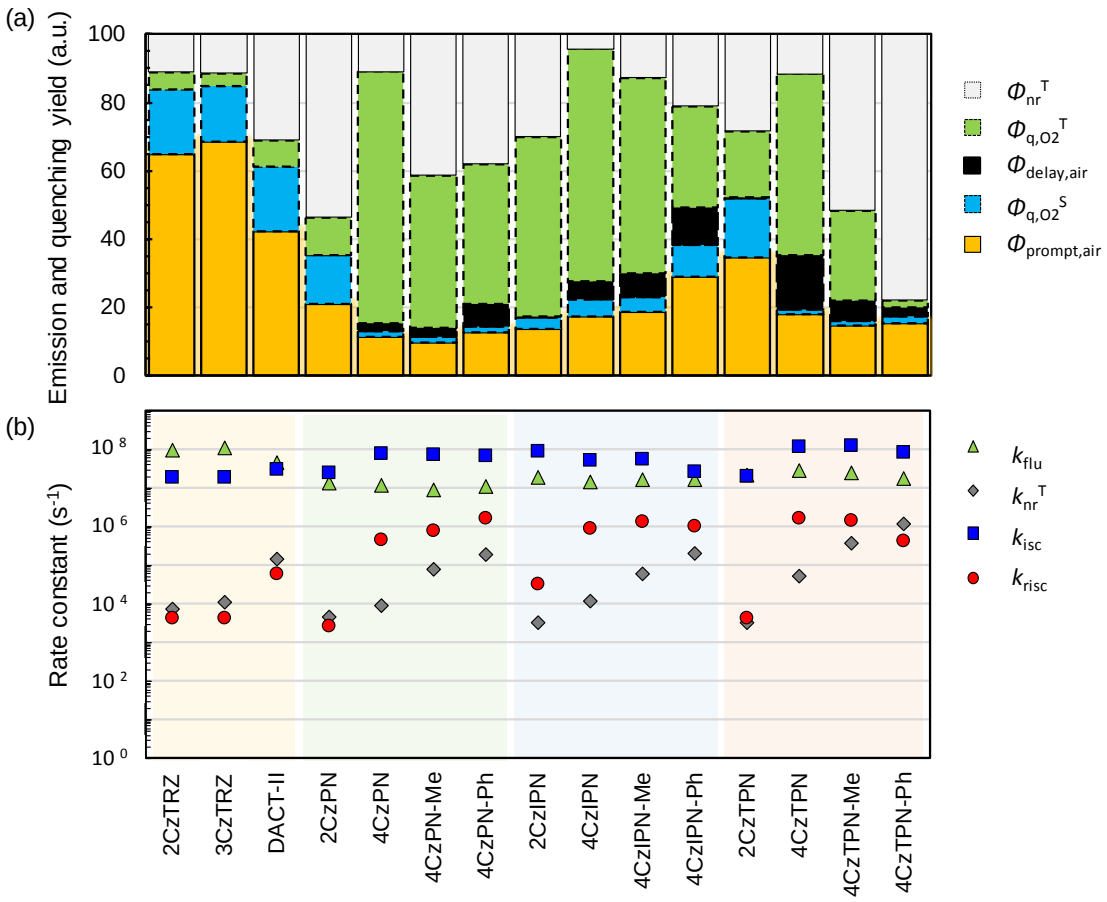

Figure 3-5. a) The deactivation process from S_1 and T_1 under air-saturated conditions and b) the activation or deactivation rate constants of the TADF materials.

$$^{1}\mathrm{M}^{*} + \mathrm{O_2} \rightarrow (\mathrm{M} \cdots \mathrm{O_2})^{*} \rightarrow \mathrm{M} + \mathrm{O_2}, \quad (3\text{-}1)$$

$$\rightarrow {}^{3}\mathrm{M}^{*} + \mathrm{O_2}\,(^{1}\Delta_g), \quad (3\text{-}2)$$

$$\rightarrow {}^{3}\mathrm{M}^{*} + \mathrm{O_2}, \quad (3\text{-}3)$$

where M^{*} indicates an excited state of an organic molecule M. As shown in **Scheme (3-2)**, O_2 is paramagnetic and known to quench fluorescence and enhance intersystem crossing (ISC) process of emitters that have larger energy gap between S_1 and T_1 levels (ΔE_{ST}) than the O_2 ($^{1}\Delta_g$) energy, which is equal to 0.98 eV.[18] Although the ΔE_{ST} of TADF emitters are not large enough to excite O_2, the rate constant of oxygen quenching under air-saturated conditions from S_1 ($k_{q,O2}^{S}$) can be competitive with the sum of k_{flu} and the

rate constant of ISC(k_{isc}) in some TADF molecules by the processes of (1) and (3) ($k_{q,O2}^{S} \approx 10^7\ s^{-1}$). These values are one order of magnitude greater than $k_{q,O2}$ from T_1 ($k_{q,O2}^{T}$) and the correlation can be explained by the spin multiplicity of CCT complexes as below:[21-22]

$$^3M^* + O_2 \rightleftarrows {}^5(M \cdots O_2)^* \quad (3\text{-}4)$$

$$\rightleftarrows {}^3(M \cdots O_2)^* \rightarrow {}^1M + O_2(^1\Delta_g) \quad (3\text{-}5)$$

$$\rightleftarrows {}^1(M \cdots O_2)^* \rightarrow {}^1M + O_2(^1\Delta_g) \quad (3\text{-}6)$$

While three different types of CCT exciplexes are given from the combination of a triplet exciton and O_2, singlet and/or triplet multiplicities, that are 1/9 to 4/9 of the total CCT exciplexes can be the main quenching channel because of the multiplicity-allowed transition (**Scheme 3-6**).

3. 2. 2. Intramolecular exciton quenching

On the basis of these results, the internal nonradiative deactivation pathways of the triplet states, $k_{nr,int}^{T}$, of carbazolyl phthalonitriles were compared with their photophysical properties. The calculated rate constants of the TADF materials are summarized in **Fig. 3-5b** and **Table 3-1**. In our previous study, the PLQY and τ_{delay} of 4CzTPN and its derivatives decreased with substitution at the 3- and 6-positions of the carbazolyl groups (**Figure ex3-2**, Appendix).[5] In the low singlet-energy region, such as red emission, exponential correlation between $k_{nr,int}^{T}$ and the energy level called the “energy gap law” was observed. **Figure 3-6** shows a plot of $k_{nr,int}^{T}$ and S_1 at room temperature (E_{S1_RT}) estimated from the onset of the fluorescence spectra. This indirect relationship between $k_{nr,int}^{T}$ and E_{S1_RT} can be explained by the fact that T_1 at room temperature (E_{T1_RT}) is close to E_{S1_RT} because of its small ΔE_{ST}, especially for group III compounds. Although

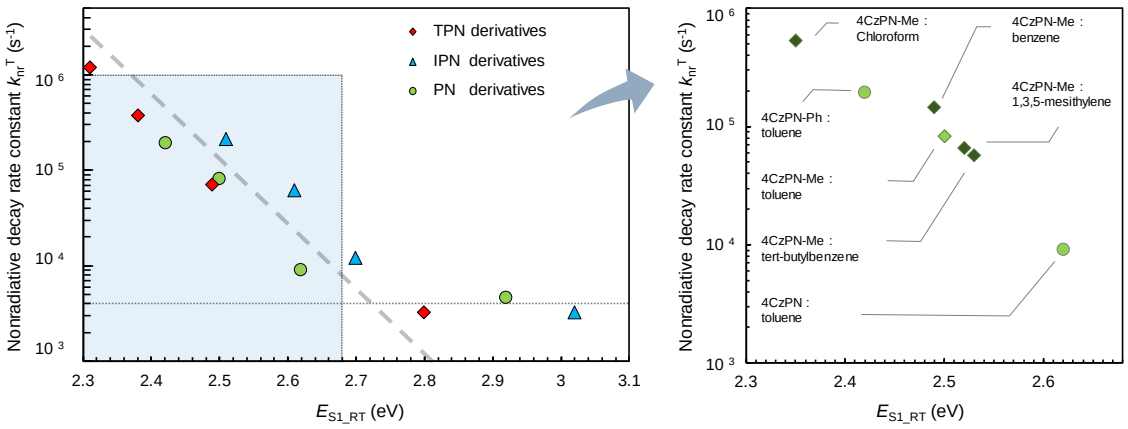

Figure 3-6. The relationship between $k_{nr,int}^T$ of carbazolyl phthalonitriles and E_{S1_RT}. Inset: $k_{nr,int}^T$ of 4CzPN-Me with different solvents

group III compounds have relatively large k_{risc} of around 10^6 s^{-1}, 4CzTPN-Ph with the lowest E_{S1_RT} has a much larger $k_{nr,int}^T$ than k_{risc}. Consequently, the molecular design of red or near-infrared TADF emitters is more difficult than that of shorter wavelength emitters.[23] In the high singlet-energy region (> 2.8 eV), $k_{nr,int}^T$ had a nearly constant value of around 10^3–10^4 s^{-1} for all emitters. This value will be caused by unexpected O_2 that remains or unwarranted penetration even after careful purging with inert gas ($[O_2] \approx 10^{-6}$–10^{-7} M) because of the diffusion rate constant in the solvent ($k_{diff} \approx 10^{10}$ s^{-1} M^{-1}). Smaller $k_{nr,int}^T$ could hardly be observed in solution measurements.

The effects of environmental conditions, such as solvent polarization, on the $k_{nr,int}^T$ were also investigated using 4CzPN-Me as a model emitter. The $k_{nr,int}^T$ of 4CzPN-Me could be clearly distinguished from the quenching characteristics of O_2. The selected solvents were benzene, 1,3,5-methytilene, *tert*-butylbenzene, and chloroform. Here, E_{S1_RT} was stabilized in accordance with the polarizability of the solvents (**Figure ex3-3**, Appendix).[24] This solvatochromism is also subject to the energy gap law likewise the effect of substitution at the 3- and 6-positions of carbazolyl groups shown in **Fig. 3-6**. External effects because of environmental changes are expected to happen in solid state-

like amorphous host–guest systems in films.

3. 3. Conclusion

In summary, I investigated intrinsic and extrinsic nonradiative deactivation pathways, especially by O_2, from the excited states of organic molecules exhibiting TADF in the presence and absence of oxygen conditions. I revealed that O_2 strongly affected the decay processes of not only triplets but also singlet excitons of TADF emitters despite its small ΔE_{ST}. To evaluate the optical characteristics of TADF molecules in solution, oxygen quenching from the exited singlet state should be considered because of competitive k_{qO2}^{S} to k_{flu} and k_{isc} processes. Compared with the conventional method, our method incorporating the effect of $k_{q,O2}^{S}$ makes it easier to evaluate the rate constants of TADF molecules even with large k_{flu}/k_{risc} ratios of over 10^4. Furthermore, TADF materials with low singlet energies are subject to the energy gap law. In toluene, $k_{nr,int}^{T}$ overcomes k_{risc} when the energy is less than 2.3 eV.

3. 4. Experimental methods

3. 4. 1. Preparation of samples

All TADF compounds were prepared as described in the literature [5,13-14] and purified by sublimation.

Sample solutions were prepared by dissolving the materials in the required solvents to a concentration of 10^{-5} M. The toluene, benzene, and chloroform were used spectroscopic grade. *tert*-butylbenzene and 1,3,5-methytilene were distillated before use. After the initial assessment of PL characteristics of the solutions, the solutions were purged with high-purity nitrogen (5N grade) in the quartz cell through the septum by a

syringe needle for 30 minutes. To prevent evaporation of the solvents, the gases were passed through the neat solvents before bubbling the solutions. After the degassing process, the quartz cell was immediately encapsulated by Parafilm®. These operations are conducted at 298 ± 1 K.

3. 4. 2. Measurement of photophysical properties

PL spectra were measured using multi-channel analyzer (PMA-12 C10027-01, Hamamatsu Photonics). O_2 ($^1\Delta_g$) emission spectra were detected from the 10^{-4} M solutions using an absolute photoluminescence quantum yield measurement system (Quantaurus-QY Plus C13534-02, Hamamatsu Photonics) with an excitation wavelength of 400 nm.

Emission lifetimes were measured using a fluorescence lifetime measurement system (Quantaurus-Tau C11367-21, Hamamatsu Photonics).

PLQY of the solutions were measured under air and purged with nitrogen gas using an absolute PLQY measurement system (Quantaurus-QY Plus C13534-02, Hamamatsu Photonics) with an excitation wavelength of 360 nm. These measurements were carried out at 298 ± 1 K. A breakdown of Φ_{total} into Φ_{prompt} and Φ_{delay} was calculated as follows:

$$\Phi_{prompt} = \Phi_{prompt} \times \tau_{prompt,N2} / \tau_{prompt,air} , \quad \text{(eq. 3-1)}$$

$$\Phi_{delay} = \Phi_{total} - \Phi_{prompt} . \quad \text{(eq. 3-2)}$$

Decay rate constants were determined by from their quantum yields and lifetimes as described in the literature.[7-8]

$$k_{prompt} = 1 / \tau_{prompt,N2} , \quad \text{(eq. 3-3)}$$

$$k_{delay} = 1 / \tau_{delay,N2} , \quad \text{(eq. 3-4)}$$

$$k_{flu} = \Phi_{prompt} \times k_{prompt} , \quad \text{(eq. 3-5)}$$

$$k_{isc} = (1 - \Phi_{prompt}) \times k_{prompt} , \quad \text{(eq. 3-6)}$$

$$k_{risc} = k_{prompt} \times k_{delay} \times \Phi_{delay} / (k_{isc} \times \Phi_{prompt}) , \quad \text{(eq. 3-7)}$$

$$k_{nr,int}{}^{T} = k_{delay} - \Phi_{prompt} \times k_{risc} . \quad \text{(eq. 3-8)}$$

Here, $k_{nr,int}{}^{S}$ is assumed to be 0 because prompt component showed virtually no temperature dependence (**Figure ex3-4**, Appendix).

3. 5. References

[1] R. S. Nobuyasu, Z. Ren, G. C. Griffiths, A. S. Batsanov, P. Data, S. Yan, A. P. Monkman, M. R. Bryce, F. B. Dias. *Adv. Optical Mater.* **2016,** *4*, 597.

[2] T. Hosokai, H. Matsuzaki, H. Nakanotani, K. Tokumaru, T. Tsutsui, A. Furube, K. Nasu, H. Nomura, M. Yahiro, C. Adachi. *Science Advances*, **2017**, *3*, e1603282.

[3] M. Saigo, K. Miyata, S. Tanaka, H. Nakanotani, C. Adachi, K. Onda. *J. Phys. Chem. Lett*. 2019, **10**, 2475.

[4] H. Noda, X.-K. Chen, H. Nakanotani, T. Hosokai, M. Miyajima, N. Noutsuka, Y. Kashima, J.-L. Bredas, C. Adachi. *Nature Mater.* **2019**, *18*, 1084.

[5] H. Uoyama, K. Goushi, K. Shizu, H. Nomura, C. Adachi. *Nature* **2012**, *492*, 234.

[6] A. Endo, K. Sato, K. Yoshimura, T. Kai, A. Kawada, H. Miyazaki, C. Adachi. *Appl. Phys. Lett.* **2011**, *98*, 083302.

[7] K. Goushi, K. Yoshida, K. Sato, C. Adachi. *Nature Photon.* **2012**, *6*, 253.

[8] K. Masui, H. Nakanotani, C. Adachi. *Organic Electron.* **2013**, *14*, 2721.

[9] T. Nakagawa, S.-Y. Ku, K.-T. Wong. C. Adachi. *Chem. Commun.*, **2012**, *48*, 9580.

[10] G. Méhes, H. Nomura, Q. Zhang, T. Nakagawa, C. Adachi. *Angew. Chem. Int. Ed.* **2012**, *51*, 11311.

[11] F. B. Dias, K. N. Bourdakos, V. Jankus, K. C. Moss, K. T. Kamtekar, V. Bhalla, J. Santos, M. R. Bryce, A. P. Monkman. *Adv. Mater.* **2013**, *25*, 3707.

[12] C. Rothe, A. P. Monkman. *Phys. Rev. B* **2003**, *68*, 075208.

[13] S. Hirata, Y. Sakai, K. Masui, H. Tanaka, S. Y. Lee, H. Nomura, N. Nakamura, M.

Yasumatsu, H. Nakanotani, Q. Zhang, K. Shizu, H. Miyazaki, C. Adachi. *Nature Mater.* **2015**, *14*, 330.

[14] H. Kaji, H. Suzuki, T. Fukushima, K. Shizu, K. Suzuki, S. Kubo, T. Komino, H. Oiwa, F. Suzuki, A. Wakamiya, Y. Murata, C. Adachi. *Nature Commun.* **2015**, *6*, 8476.

[15] N. Hasebe, K. Suzuki, H. Horiuchi, H. Suzuki, T. Yoshihara, T. Okutsu, S. Tobita. *Anal. Chem.* **2015**, *87*, 2360.

[16] R. J. Vázquez, H. Kim, P. M. Zimmerman, T. Goodson III. *J. Mater. Chem. C*, **2019**, *7*, 4210.

[17] K. Gollnick, G. O. Schenck. *Pure Appl. Chem.* **1964**, *9*, 507.

[18] A. J. McLean, D. J. McGarvey, T. G. Truscott, C. R. Lambed, E. J. Land. *J. Chem. Soc., Faraday Trans.*, **1990**, *86*, 3075.

[19] K. Kikuchi, C. Sato, M. Watanabe, H. Ikeda, Y. Takahashi, T. Miyashi, *J. Am. Chem. Soc.* **1993**, *115*, 5180.

[20] A. A. Adbel-Shafi, D. R. Worrall. *J. Photochem. Photobiol. A Chem.* **2005**, *172*, 170.

[21] M. Okamoto, F. Tanaka, S. Hirayama. *J. Phys. Chem. A* **1998**, *102*, 10703.

[22] D. H. Volman, G. S. Hammond, K. Gollnick, Advances in Photochemistry Volume 14, **1988**.

[23] J. H. Kim, J. H. Yun, J. Y. Lee. *Adv. Optical Mater.* **2018**, *6*, 1800255.

[24] M. Aroney, S. J. Pratten. *J. Chem. SOC., Faraday Trans. I*, **1984**, *80*, 1201.

Chapter 4

Summary of this thesis and future perspectives

4. 1. Summary of this thesis

In this thesis, I investigated nonradiative deactivate phenomena which compete with the emission pathways in LL-RTP and TADF emitters as summarized in **Figure 4-1**.

In Chapter 2, the quenching factors of LL-RTP emitters in organic semiconducting hosts were studied. Oxygen quenching rate constant in organic semiconducting solid-state films was determined to be around 10^3 s^{-1}. This value is smaller than that in solution, but quite larger than the rate constant of phosphorescence (k_{phos}) of LL-RTP emitters. Other quenching factors were also investigated by changing the photophysical properties of the host materials in the absence of O_2. Under room temperature, an endothermic energy transfer from an emitter to a host matrix was observed even with $\Delta E_{T1\text{-}T1'}$ larger than 0.3 eV. The nonradiative rate constants of some host matrices, $k_{nr,host}^{T}(RT)$, were exceeded 10^0 s^{-1}, leading to the quenching of guest phosphorescence.

In Chapter 3, quenching behaviors of TADF emitters in diluted solutions were studied. Under the air-saturated condition, oxygen quenching rate constants for triplet excitons of TADF molecules ($k_{q,O2}^{T}$) in toluene solution were determined to be around 10^6 s^{-1}. This value is one order of magnitude smaller than that of the singlet excitons ($k_{q,O2}^{S} \sim 10^7$ s^{-1}). Thus, some TADF molecules have a comparative rate constant of the prompt component, k_{prompt} (= k_{flu} + k_{isc}), with $k_{q,O2}^{S}$, resulted in a partial quenching of the singlet emission. Further, the rate constants of reverse intersystem crossing (k_{risc}) of TADF emitters were observed in the range of $k_{risc} = 10^3$ to 10^6 s^{-1}. Thus, according to the "energy gap law", I confirmed that k_{risc} can be defeated by the rate constant of nonradiative deactivation $k_{nr,int}^{T}$ when the energy is less than 2.3 eV.

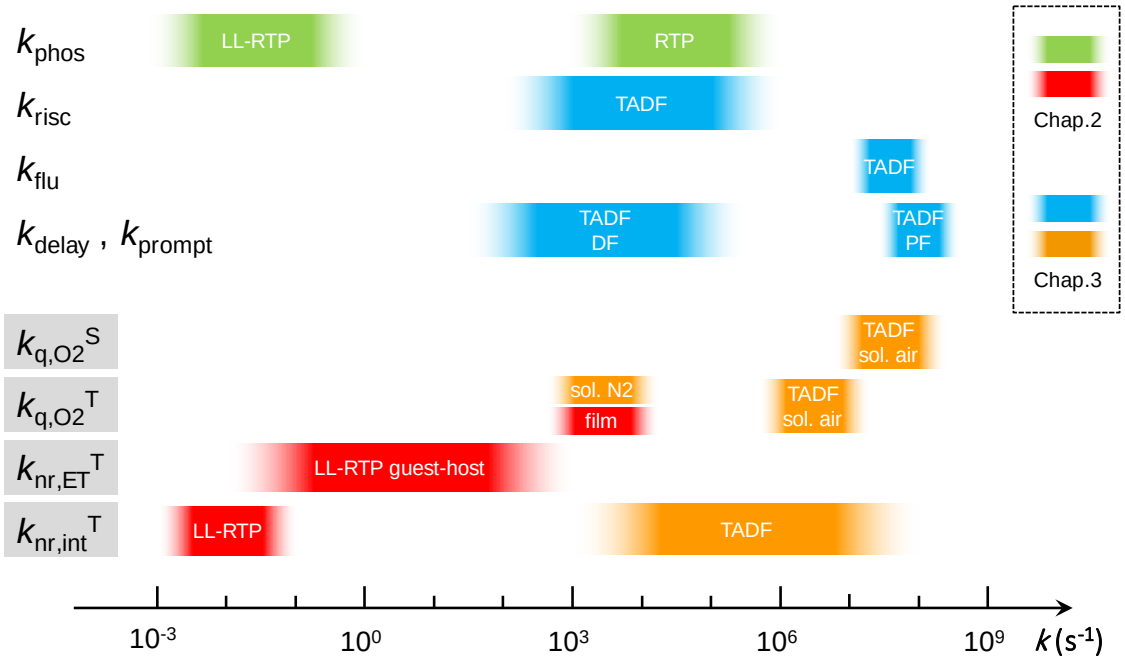

Figure 4-1. Radiative or nonradiative rate constants studied in this thesis.

4. 2. Future perspective

Finally, I mention the future perspective of further triplet harvesting based on my experimental results.

For LL-RTP emitters, the maximum lifetime length is intrinsically limited by $1/k_{phos}$ and the long lifetime triplets would induce reverse energy transfer to a host matrix or upconversion into a singlet state. Thus, to obtain longer afterglow EL from OLEDs, other novel scheme should be considered. For example, incorporating "organic long persistent luminescence" (OLPL)[1] inspired by inorganic carrier trapping/de-trapping systems is one of the possible candidates.

In particular, to realize highly efficient deep-red TADF emission, the design of TADF molecules and OLEDs should incorporate further advanced concepts. For example, the material having the adjusted localized excited (LE) triplet energy level as T_1 [2] can reduce the nonradiative deactivation from the triplet states. (**Figure 4-2**a). T_1 (LE) usually has smaller $k_{nr,int}^{T}$ than T_1 (CT) due to the small transition factors of f_s, and f_v. For example, non-deuterated DPADPC (DPADPC-h_{25}) in Chapter 2, using a dibenzo[g,p]chrysene unit, exhibited $k_{nr,int}^{T}(RT) = 5.9 \times 10^{-1}$ s^{-1} even with E_{T1} = 2.2 eV. Thus, the construction of TADF molecule with the $E_{Tn}(CT) > E_{T1}(LE)$ energy level would realize highly efficiency deep-red emitters. Further, the use of a TADF-assisted fluorescence (TAF) system[3-4] is also promising to enable deep-red emission (**Fig. 4-2**b). A TAF system can transfer the energy from S_1 of a TADF molecule to S_1 of a conventional fluorescent molecule. This can convert a dark triplet to a bright singlet without facing the problem of energy gap law.

Finally, I wish that the TADF measurement technique proposed in this thesis will accelerate the screening of TADF materials, leading to the rapid development for the practical use.

(a) Approach I

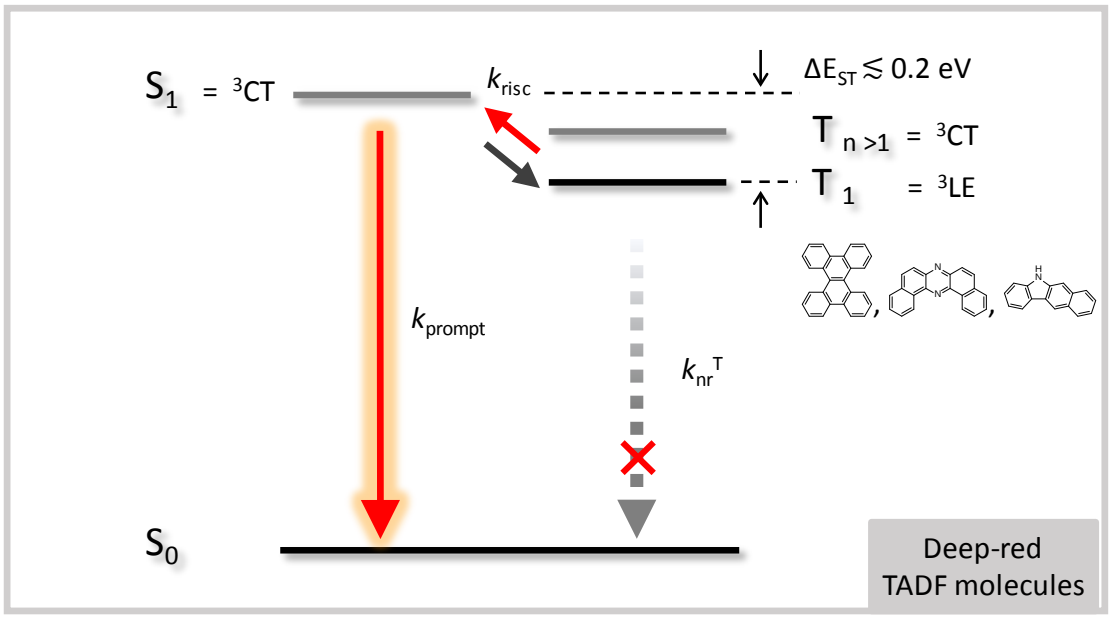

(b) Approach II

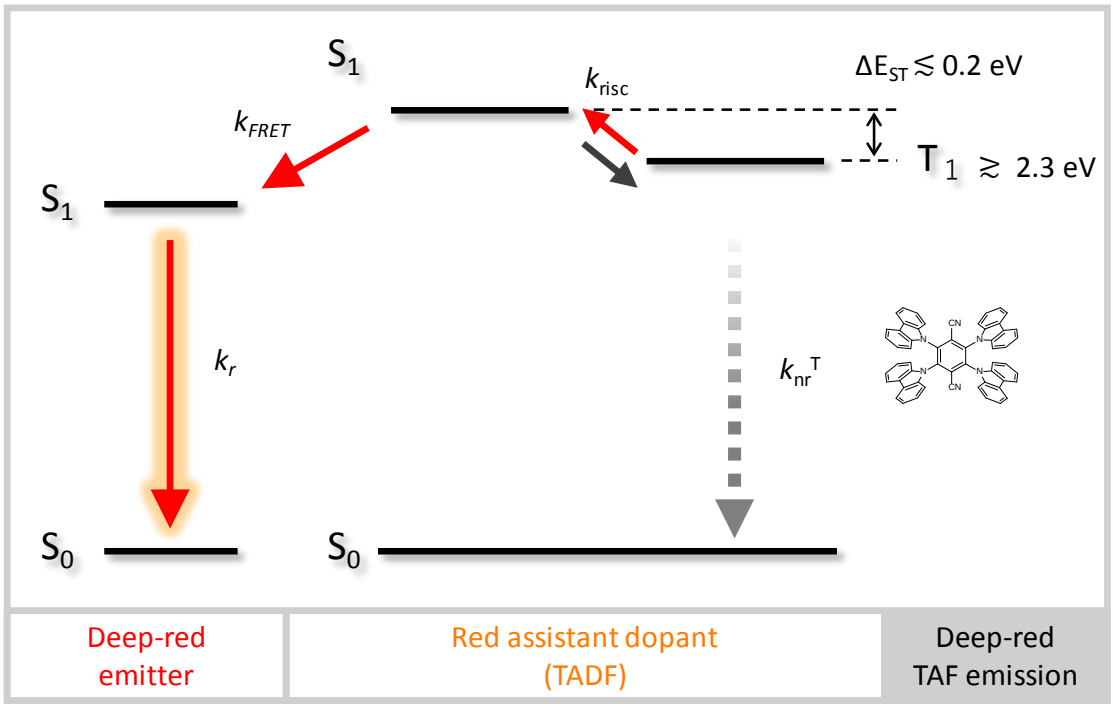

Figure 4-2. Approach to obtain deep-red luminescence using TADF emitter. a) ^{3}(LE) is lower than ^{3}(CT). b) TAF system with energy transfer mechanism from TADF emitter into fluorescent emitter.

4. 3. References

[1] R. Kabe, C. Adachi, *Nature* **2017**, *550*, 384.

[2] P. Data, P. Pander, M. Okazaki, Y. Takeda, S. Minakata, A. P. Monkman, *Angew. Chem. Int. Ed.* **2016**, *55*, 5739.

[3] H. Nakanotani, T. Higuchi, T. Furukawa, K. Masui, K. Morimoto, M. Numata, H. Tanaka, Y. Sagara, T. Yasuda, C. Adachi, *Nature Commun.* **2014**, *5*, 4016.

[4] T. Yamanaka, H. Nakanotani, S. Hara, T. Hirohata, C. Adachi, *Appl. Phys. Express* **2017**, *10*, 074101.

Appendix

Materials in this thesis

Chapter 2

2-MeTHF: 2-methyltetrahydrofuran

Coronene

DMFLTPD: 9,9-dimethyl-*N*^{2},*N*^{7}-diphenyl-*N*^{2},*N*^{7}-di-m-tolyl-9*H*-fluorene-2,7-diamine

DPADBC: *N*,*N*-diphenyldibenzo[g,p]chrysen-2-amine

DPEPO: bis[2-((oxo)diphenylphosphino)phenyl]ether

ITO: Indium tin oxide

$Ir(ppy)_3$: tris(2-phenylpyridinato)iridium(III)

LiF: Lithium fluoride

PPT: dibenzo[b,d]thiophene-2,8-diylbis(diphenylphosphine oxide)

mCP: 1,3-di(9*H*-carbazol-9-yl)benzene

mCBP: 3,3'-di(9*H*-carbazol-9-yl)-1,1'-biphenyl

PtOEP: Platinum octaethylporphyrin

TPD: *N*^{4},*N*^{4}'-diphenyl-*N*^{4},N^4'-di-m-tolyl-[1,1'-biphenyl]-4,4'-diamine

TrisPCz: 9,9',9''-triphenyl-9*H*,9'*H*,9''*H*-3,3':6',3''-tercarbazole

α-NPD: *N*^{4},*N*^{4}'-di(naphthalen-1-yl)-*N*^{4},*N*^{4}'-diphenyl-[1,1'-biphenyl]-4,4'-diamine

β-estradiol

Chapter 3

1,3,5-Mesthylene

2CzIPN: 4,6-di(9*H*-carbazol-9-yl)isophthalonitrile

2CzPN: 4,5-di(9*H*-carbazol-9-yl)phthalonitrile

2CzTPN: 2,5-di(9*H*-carbazol-9-yl)terephthalonitrile

4CzIPN: 2,4,5,6-tetra(9*H*-carbazol-9-yl)isophthalonitrile

4CzIPN-Me: 2,4,5,6-tetrakis(3,6-dimethyl-9*H*-carbazol-9-yl)isophthalonitrile

4CzIPN-Ph: 2,4,5,6-tetrakis(3,6-diphenyl-9*H*-carbazol-9-yl)isophthalonitrile

4CzPN: 3,4,5,6-tetra(9*H*-carbazol-9-yl)phthalonitrile

4CzPN-Me: 3,4,5,6-tetrakis(3,6-dimethyl-9*H*-carbazol-9-yl)phthalonitrile

4CzPN-Ph: 3,4,5,6-tetrakis(3,6-diphenyl-9*H*-carbazol-9-yl)phthalonitrile

4CzTPN: 2,3,5,6-tetra(9*H*-carbazol-9-yl)terephthalonitrile

4CzTPN-Me: 2,3,5,6-tetrakis(3,6-dimethyl-9*H*-carbazol-9-yl)telephthalonitrile

4CzTPN-Ph: 2,3,5,6-tetrakis(3,6-diphenyl-9*H*-carbazol-9-yl)telephthalonitrile

Benzene

Chloroform

DACT-II: 9-(4-(4,6-diphenyl-1,3,5-triazin-2-yl)phenyl)-N^3,N^3,N^6,N^6-tetraphenyl-9*H*-carbazole-3,6-diamine

2CzTRZ: 9-(4-(4,6-diphenyl-1,3,5-triazin-2-yl)phenyl)-9*H*-3,9'-bicarbazole

3CzTRZ: 9'-(4-(4,6-diphenyl-1,3,5-triazin-2-yl)phenyl)-9'*H*-9,3':6',9''-tercarbazole

tert-Butylbenzene

Toluene

Detailed data in this thesis

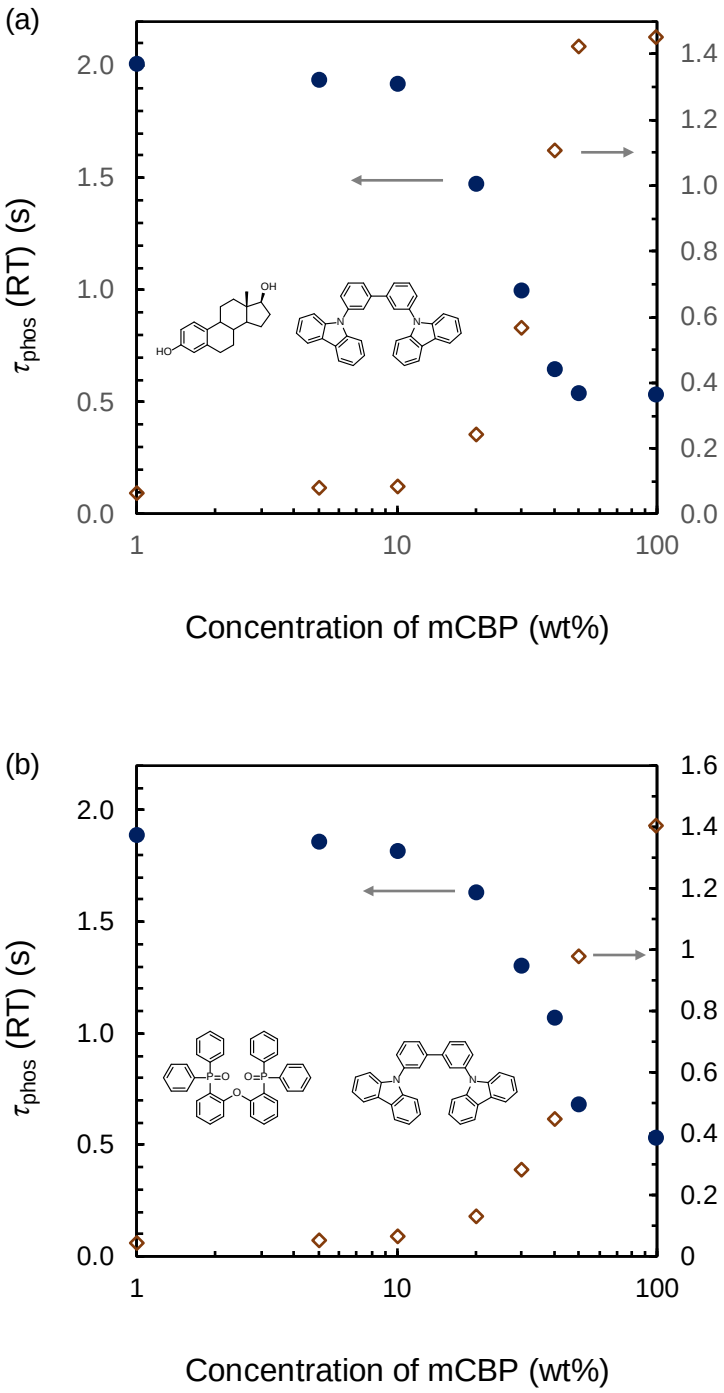

Figure ex2-1. Relationship between τ_{phos}(RT) or k_{nr}^{T}(RT) of DMFLTPD-d_{36} and the doping concentration of mCBP in (a) β-estrasiol/mCBP (b)DPEPO/mCBP mixed matrices.

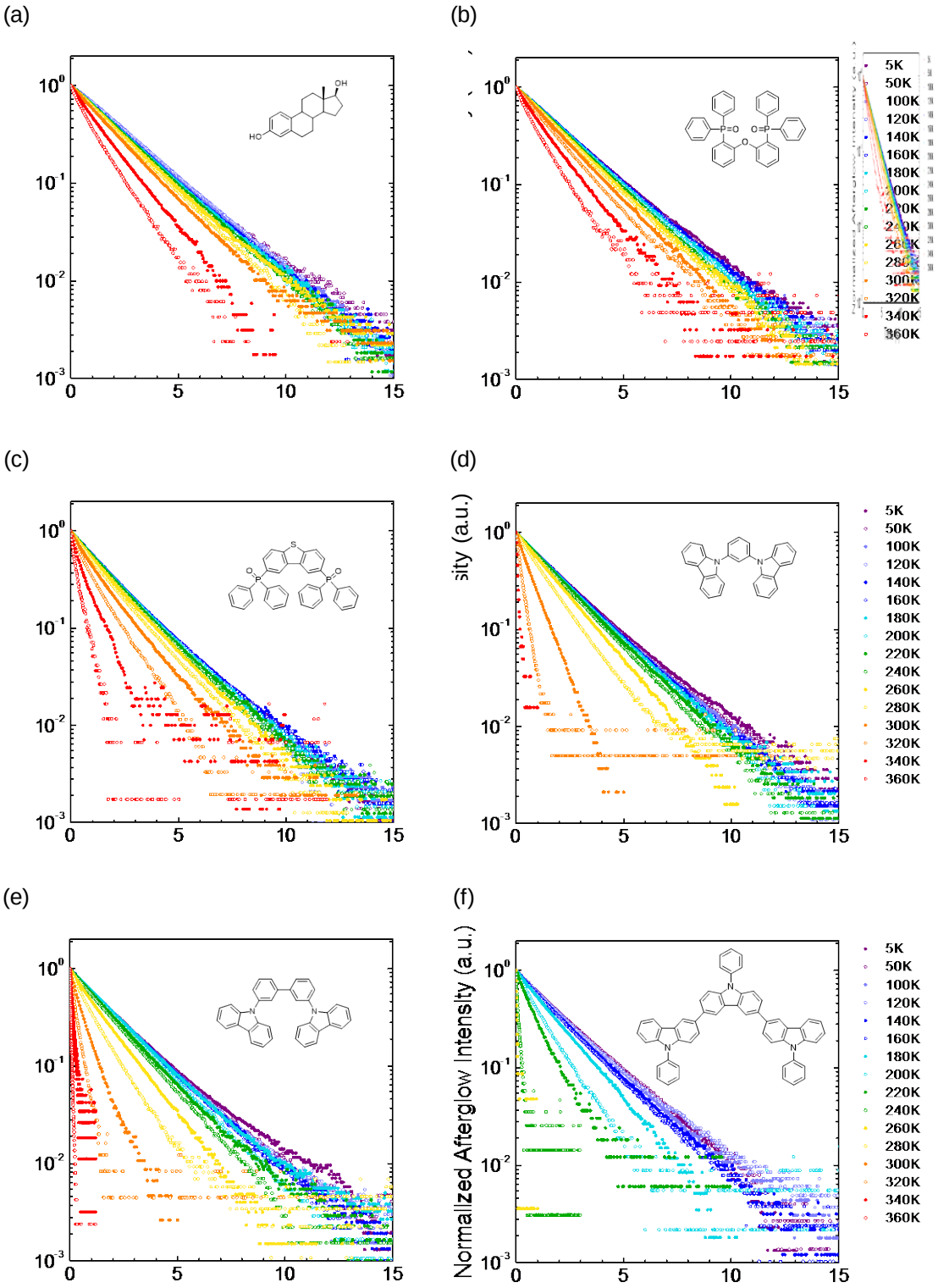

Figure ex2-2. Temperature dependent transient phosphorescence decay curves of DMFLTPD-d_{36} films.

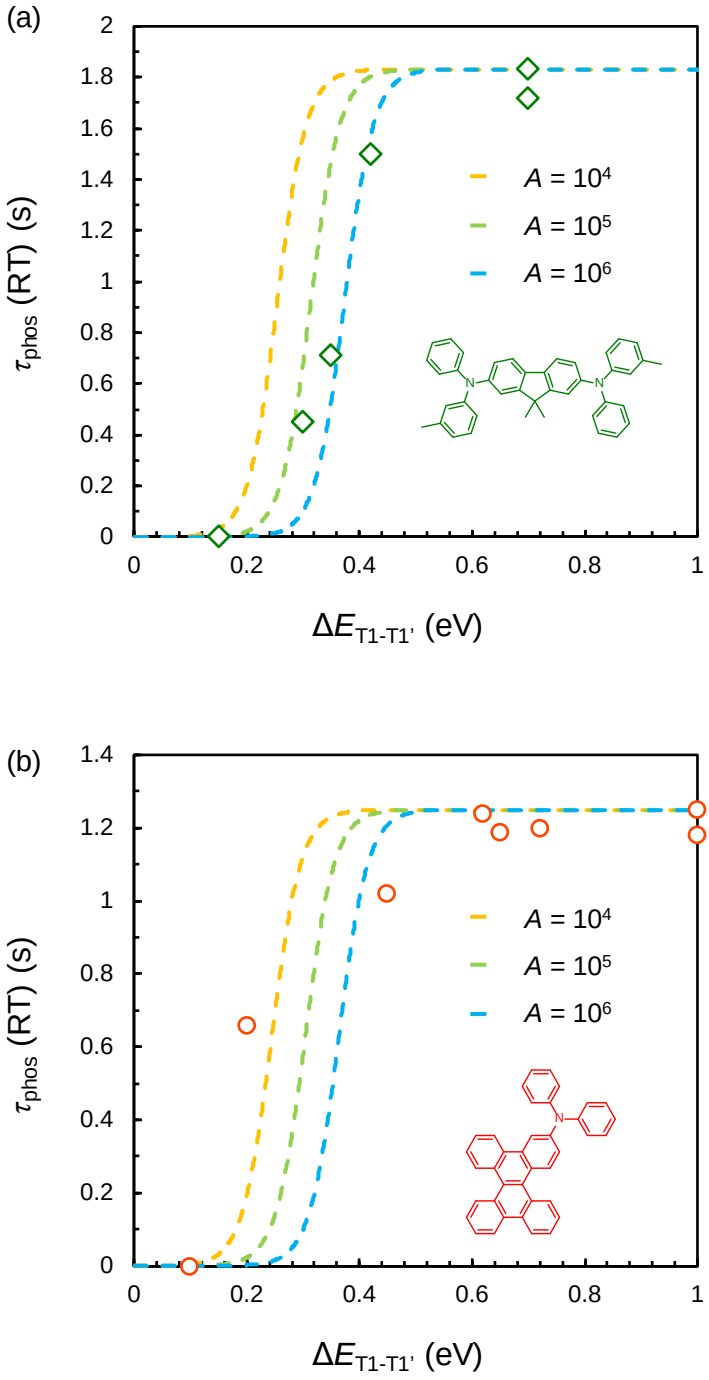

Figure ex2-3. Relationship between τ_{phos}(RT) and $\Delta E_{T1\text{-}T1'}$ using a) DMFLTPD-d_{36} or b) DPADBC-d_{25} as the guest with the fitting curves (dotted).

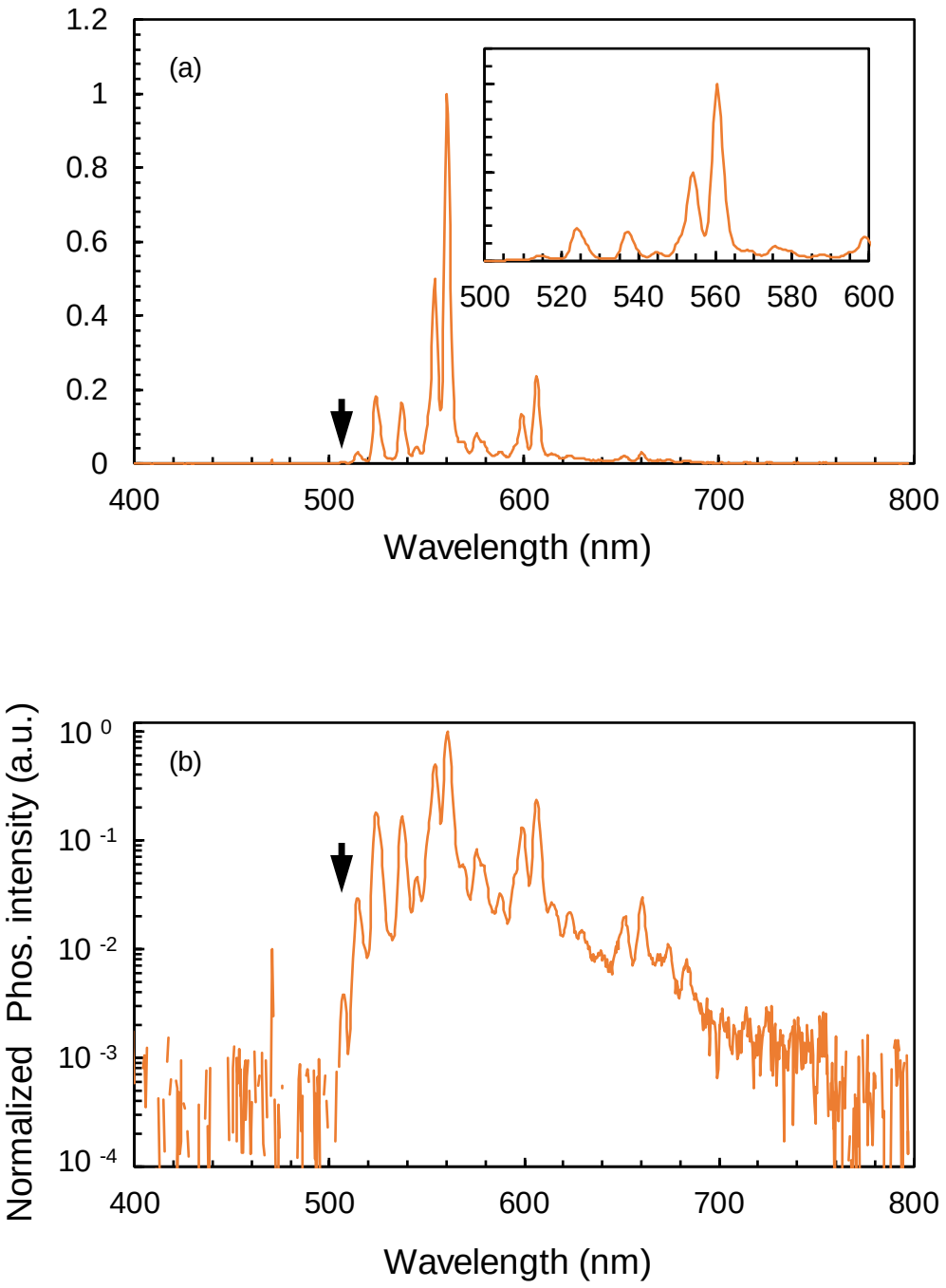

Figure ex2-4. Phosphorescence spectra of coronene-d_{12} in frozen 2-MeTHF at 77K on a) linear and b) log scales.

Detailed data in Chapter 3

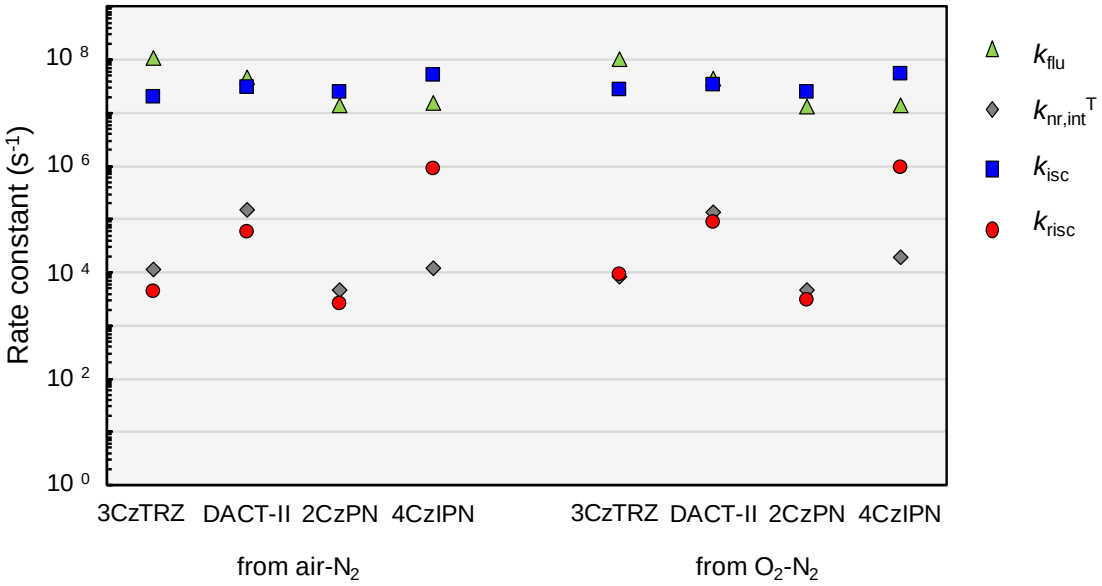

Figure ex3-1. Comparison of the rate constants of TADF materials in toluene using different O_2 present conditions. Under air-saturated condition (left) and O_2-purged condition (right).

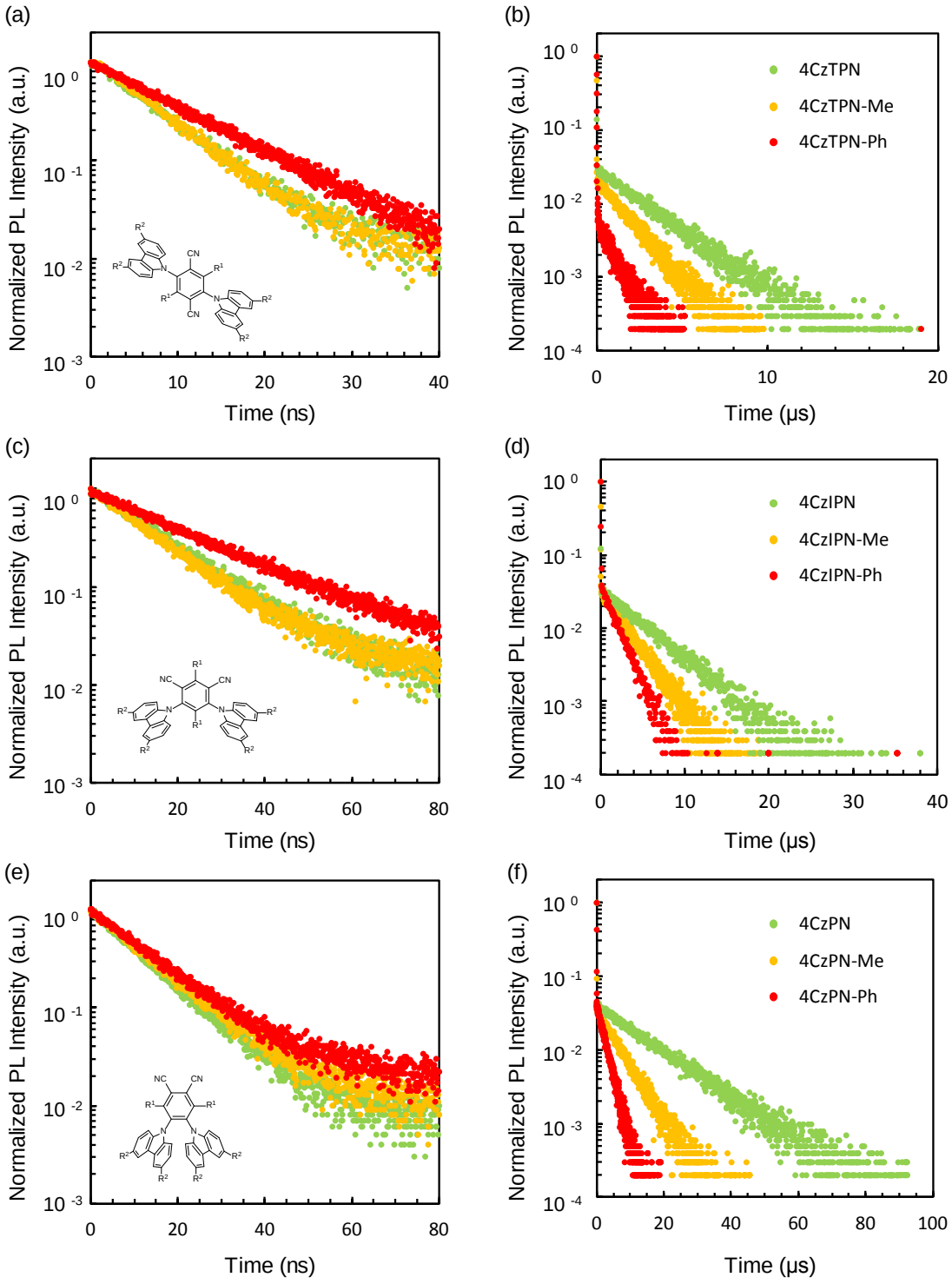

Figure ex3-2. Transient PL decay profiles of the prompt component (left column) and delayed component (right column) of a) 4CzTPN derivatives, b) 4CzIPN derivatives, and c) 4CzPN derivatives.

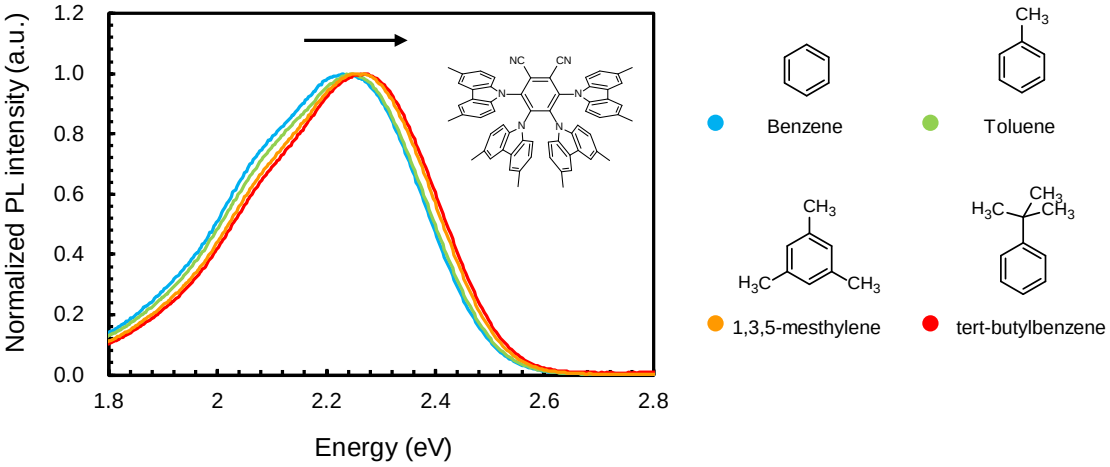

Figure ex3-3. Solvent-dependent spectral shift of 4CzPN-Me.

(a) 4CzPN-Me :

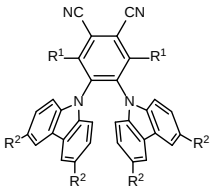

R^1 = 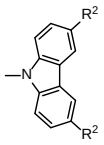 , R^2 = Me

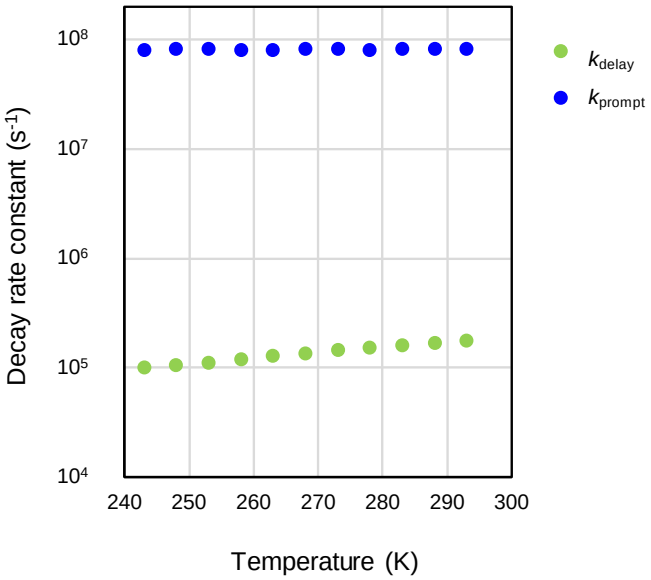

(b) 4CzIPN-Me :

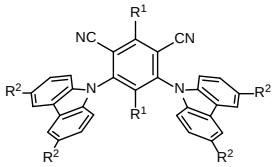

R^1 = 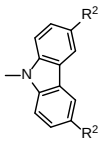 , R^2 = Me

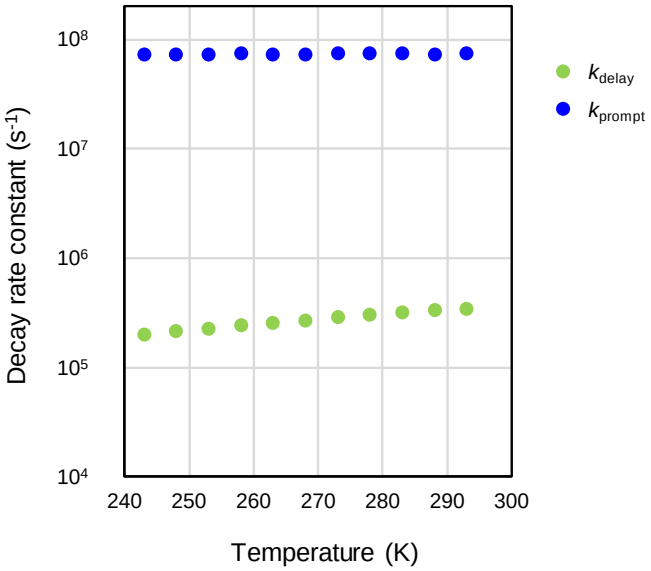

Figure ex3-4. Temperature dependence of the prompt and delayed rate constants of 4CzIPN-Me and 4CzPN-Me in toluene.

Publication list

Original papers

1) Ryota Kabe, **Naoto Notsuka**, Kou Yoshida, Chihaya Adachi, *Advanced Materials* **2016**, *28*, 655-660.
"Afterglow Organic Light Emitting Diodes"

2) **Naoto Notsuka**, Ryota Kabe, Kenichi Goushi, Chihaya Adachi, *Advanced Functional Materials* **2017**, *27*, 40, 1703902.
"Confinement of Long-Lived Triplet Excitons in Organic Semiconducting Host-Guest Systems"

3) **Naoto Notsuka**, Hajime Nakanotani, Hiroki Noda, Kenichi Goushi, Chihaya Adachi. *Journal of Physical Chemistry Letters* DOI: 10.1021/acs.jpclett.9b03302.
"Observation of Nonradiative Deactivation Behavior from Singlet and Triplet States of Thermally Activated Delayed Fluorescence Emitters in Solution"

Joint papers

1) Hiroyuki Mieno, Ryota Kabe, **Naoto Notsuka**, Mark D Allendorf, Chihaya Adachi, *Advanced optical Materials* **2016**, *4*, 7, 1015-1021.
"Long-Lived Room-Temperature Phosphorescence of Coronene in Zeolitic Imidazolate Framework ZIF-8"

2) Hiroki Noda, Xian-Kai Chen, Hajime Nakanotani, Takuya Hosokai, Momoka Miyajima, **Naoto Notsuka**, Yuuki Kashima, Jean-Luc Brédas, Chihaya Adachi, *Nature Materials* **2019**, *18*, 1084-1090.
"Critical role of intermediate electronic states for spin-flip processes in charge-transfer-type organic molecules with multiple donors and acceptors"

List of presentations at international conferences

1) **Naoto Notsuka**, Ryota Kabe, Chihaya Adachi,
International Chemical Congress of Pacific Basin Societies, December 17, 2015, Hawaii, USA.
"Long-lived phosphorescence based organic light-emitting diodes"

2) **Naoto Notsuka**, Ryota Kabe, Kenichi Goushi, Chihaya Adachi,
9th Asian Conference on Organic Electronics, October 25, 2017, Daejeon, Korea.
"Confinement of Long-Lived Triplet Excitons in Organic Semiconducting Host–Guest System"

Acknowledgments

The studies in this thesis were carried out at Adachi Laboratory, Department of Chemistry and Biochemistry, Graduate School of Kyushu University in 2014-2020.

Firstly, I am deeply grateful to Professor Chihaya Adachi for supervising this thesis, excellent experimental environment, helpful discussion, and exact comments and advice for all of my works and life.

I am also deeply grateful to Professor Hiroyuki Furuta and Professor Noritada Kaji for co-supervising of this thesis. They provided very insightful comments and suggestions, which have greatly helped me further improve the quality of this thesis.

I want to thank Associate Professor Hajime Nakanotani, Assistant Professor Kenichi Goushi, Associate Professor Ryota Kabe, and Professor Takuma Yasuda for the helpful discussions and supporting my research activities. Dr. William J. Potscavage Jr. gave me useful advice and helped in preparing my papers. I owe very important debts to Dr. Kou Yoshida and Dr. Munetomo Inoue. They kindly supported me a lot despite being busy with their studies. I would also like to thank Ms. Keiko Kusuhara and Ms. Nozomi Nakamura for the synthesis and measuring fundamental properties of materials especially in Chapter 2. I also thanks Mr. Kazuya Jinnai for supporting me on how to use the measurement systems when revising the second paper. I also acknowledge Dr. Cheok-Lam Wong, Dr. Hiroaki Ozawa, and Ms. Momoko Morio, for providing the samples, Dr. Mitsuharu Noto and Ms. Hitomi Yamamoto for the construction of the measurement systems, Dr. Hiroo Fukunaga for the valuable discussions, and Mr. Ryo Nagata and Mr. Naohiro Nishimura for helpful experiments in Chapter 3. Associate Professor Youichi Tsuchiya helped me to study my unpublished works. Mr. Hiroshi Miyazaki, Ms. Yumi Sakai, Associate Professor Masatsugu Taneda, Assistant Professor Katsuyuki Shizu, Dr.

Hiroyuki Tanaka, Mr. Yuta Sagara, Mr. Takahiro Higuchi, Dr. Hiroki Noda and Ms. Hiroko Nomura gave me valuable comments that deepen my understanding of OLEDs and photochemistry. I also acknowledge all the members of the Adachi Laboratory and all persons who I met through my works for their supports not only for my work but also for my daily life. Especially, I would thank the members of the supporting office in the laboratory.

I would also like to express my gratitude to Kyulux, Inc. for giving me generous support for my doctoral course.

Finally, I would also like to express my gratitude to my family for their moral support and warm encouragement.

January 2020 Naoto Notsuka